ACS OMEGA

Open Access

http://pubs.acs.org/journal/acsodf

Article

Hyperbranched-Polyethylenimine-Functionalized Coal Fly Ash as an Adsorbent for the Removal of Hexavalent Chromium and Reuse as a Dye Photocatalyst

Molahlegi Orienda Sebabi, Nonhlangabezo Mabuba, Kriveshini Pillay, and Soraya Phumzile Malinga*

Cite This: *ACS Omega* 2024, 9, 8954–8972

Read Online

ACCESS | Metrics & More | Article Recommendations | Supporting Information

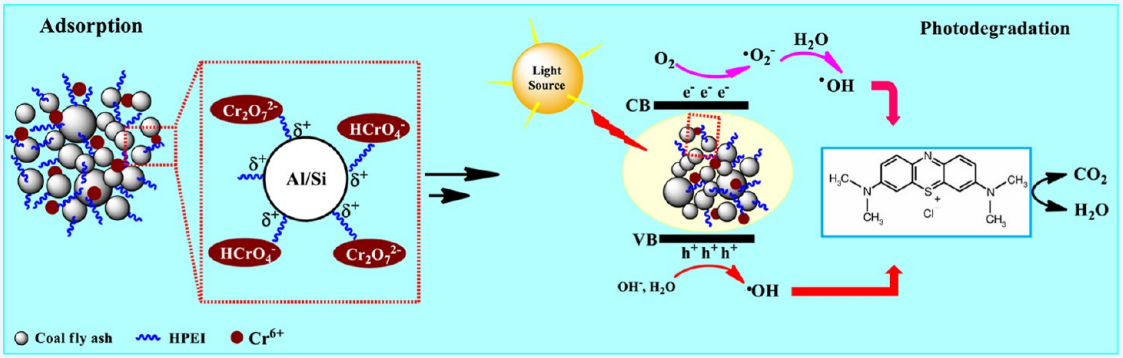

ABSTRACT: Coal fly ash (CFA) has been extensively researched as an adsorbent for heavy metals, but its application is limited by its low adsorption capacity. The modification of CFA with hyperbranched polymers results in improved adsorption capacities. Hyperbranched polyethylenimine (HPEI) is a hyperbranched polymer containing NH_2 groups that can bind with heavy metal ions through complexation or electrostatic interactions. In this study, CFA−HPEI adsorbents with various HPEI loadings (1−5%) were prepared and evaluated for the removal of Cr(VI). The successful incorporation of HPEI onto CFA was confirmed using Fourier transform infrared, elemental analysis, and X-ray photoelectron spectroscopy (XPS). The 3% CFA−HPEI loaded adsorbent resulted in optimum results when the effect of pH and adsorbent dosage was studied. The pseudo-second-order kinetics model best described the adsorption kinetics at an initial concentration of 20 mg/L. The Freundlich adsorption isotherm model best fitted the equilibrium adsorption data with a maximum adsorption capacity of 85.93 mg/g. The Cr-loaded adsorbent was reused as a photocatalyst to degrade methylene blue (MB) in the presence of visible light. The loaded adsorbent degraded 98.9% of MB (5 mg/L) within 180 min and was accompanied by compounds with m/z of 173 and 234, corresponding to the intermediate degradation of Azure A. The XPS analysis confirmed the coexistence of Cr(III) and Cr(VI) on the surface of the adsorbent. In addition, the loaded adsorbent exhibited good stability following MB degradation with no structural changes observed. Thus, CFA−HPEI adsorbents can be utilized as low-cost adsorbents for the remediation of toxic Cr(VI) from water and wastewater. The Cr-loaded CFA−HPEI adsorbent can be effectively reused as a photocatalyst, thus reducing environmental pollution.

1. INTRODUCTION

Water pollution due to heavy metals is one of the major problems currently facing the world. Effluent from a municipal wastewater treatment was found to contain Cu (0.18 mg/L), Zn (0.16 mg/L), and Pb (0.19 mg/L), which were above the permissible limits set for wastewater treatment plant effluent. Thus, the quality of the effluent that was released into the nearby river was severely impacted by this.[1] The presence of Cr(VI) in water and wastewater is a great threat due to its toxic and carcinogenic nature.[2] The main causes of Cr(VI) pollution are divided into two categories, namely, anthropogenic sources (industrial and agricultural activities, landfills, fuel combustion, and mineral processing) and natural sources (volcanic eruptions and weathering of rocks and minerals).[3] In comparison to Cr(III), hexavalent chromium [Cr(VI)] compounds are known to be more soluble and mobile in aqueous media.[4] Since Cr(VI) is a strong oxidizing agent, it can easily diffuse through cell membranes and oxidize biological molecules.[5,6] Pollution of water bodies due to Cr(VI) may result in different health complications like chronic ulcers, hemorrhage, cancer, kidney damage, nervous system failure, and dermatitis.[7,8] The United

Received: September 18, 2023
Revised: December 27, 2023
Accepted: January 10, 2024
Published: February 12, 2024

States Environmental Protection Agency recommends permissible limits of 0.5 mg/L in industrial effluent for Cr(VI).[9]

Several techniques have been applied to remove toxic heavy metals from water and wastewater. These comprise chemical coagulation, electrochemical treatment, flocculation, precipitation, reverse osmosis, biological processes, γ radiation, photo catalysis, and adsorption.[10] The utilization of most of these processes is limited by either the cost of operation or the formation of unwanted byproducts.[11] One of the most effective techniques for treating water is adsorption through low-cost adsorbents; this is because the adsorbents are inexpensive, efficient, simple to use, and easy to operate. High-quality activated carbon is still an expensive material despite its widespread use as an adsorbent in water and wastewater treatment plants. Low-cost adsorbents can be derived from natural materials (such as chitosan, zeolites. and clays), agricultural wastes (such as straw, bark, grout, seeds, peels, biochar, and biorefinery wastes), and industrial wastes [such as bagasse fly ash, slags, and coal fly ash (CFA)]. These adsorbents have drawn attention as they are (i) available locally, (ii) can be activated using low-cost and accessible reagents, and (iii) have high adsorption efficiencies. They possess a wide array of properties, which are significant for the removal of different pollutants from water and wastewater. For instance, chitosan, a linear polysaccharide, contains numerous hydroxyl groups, which act as adsorption sites for the removal of heavy metal ions. On the other hand, zeolites contain aluminum silicates, which induce properties for ion exchange and specific pore size which are crucial in the adsorption of heavy metals. Biochar, a carbon-based material resulting from the pyrolysis of biomass also attracted attention due to the presence of carboxyl and hydroxyl groups, which play a role in adsorption through ion exchange and electrostatic attraction.[12] These low-cost adsorbents have all been studied for their capability to remove toxic chemicals from water and wastewater.[13] Yogeshwaran and Priya (2021) used sugar cane bagasse for the removal of Cr(VI), Pb(II), and Zn(II) from water. High removal rates of the targeted heavy metals were observed at 95.65, 87.26, and 83.32% for Cr(VI), Pb(II), and Zn(II), respectively.[14] Sugar cane bagasse mainly contains −OH groups from cellulose and hemicellulose, which facilitates adsorption through electrostatic attraction between the adsorbent and the positively charged heavy metal ions. In line with the latter study, bentonite clay was studied for the removal of Pb(II) and Cu(II) ions from wastewater. The results attained in this study indicated that bentonite could remove up to 87.7 and 89.0% of Pb^{2+} and Cu^{2+}, respectively. The high removal rates of the targeted heavy metals were attributed to the presence of aluminum silicates in the bentonite clay. The adsorption process was mainly driven by the ion exchange between negatively charged aluminum and positively charged heavy metal ions.[15] Studies have shown that CFA can also be utilized in different applications such as in agriculture and also as an emulsifier. Adilbekova et al. (2023) modified CFA with Tween 20 and effectively applied the modified CFA as an emulsifier for water-in-oil emulsions due to its negatively charged surface, which is capable of attracting positively charged N atoms of asphaltene molecules thereby destabilizing the thin film causing the water droplets to combine.[16] The CFA modified with humic substances displayed good properties when applied in biological cultivations as soil conditioner due to the slow release of the humic substances during washing and the presence of the microbes in the material. The humic substances act as ligands for bioinorganic applications, which facilitates soil conditioning.[17]

In this study, CFA was applied because it is composed of Al_2O_3, SiO_2, Fe_2O_3, CaO, MgO, and carbon for adsorption of Cr(VI). Its physical properties such as porosity, particle size distribution, and surface area are also crucial for the adsorption process.[18−20] Although the direct application of CFA is beneficial for remediation of water from pollutants, it is limited by its low adsorption capacity and selectivity toward the analyte. Chemical modification of CFA involves the addition of functional groups on the surface of fly ash particles, thereby increasing its chemical reactivity or easy functionalization with other compounds to increase the density of surface-active sites. Different compounds have been evaluated for the activation and functionalization of CFA toward the removal of different pollutants from water and wastewater. These include metal oxides, carbon-based compounds, and amines. The effectiveness of Fe_3O_4-loaded fly ash composite for the remediation of Congo red dye from water was investigated. The Fe_3O_4-loaded fly ash composite was found to possess better magnetic characteristics, which resulted in improved adsorption capacity when compared with that of raw CFA and NaOH-treated CFA.[21] Carbon-based compounds such as amine, polydopamine, and β-cyclodextrin were used to modify CFA to prepare polydopamine-β-cyclodextrin−CFA composite for the remediation of uranium from water. The maximum adsorption capacity of 536.7 mg/g was obtained with the removal efficiency of 95.6% at pH 5.0 through complexation, hydrogen bonding, and electrostatic interaction.[22] On the other hand, CFA functionalized with amines such as 3-aminopropyltriethoxysilane have been applied for the adsorption of Cr(VI) from wastewater. Optimum adsorption conditions were obtained at pH 2 with a maximum adsorption capacity of Cr(VI) of 498.39 mg/g. The removal of Cr(VI) was found to be through electrostatic attraction between the protonated NH_3^+ of NH_2−FAT and negatively charged $HCrO_4^-$.[23]

Hyperbranched polyethylenimine (HPEI), an imine-based hyperbranched polymer consisting of a diatomic core, interior branching units of polyethylenimine, and peripheral NH_2 functional groups, has been used to functionalize different adsorbents to enhance their performance. Zeng et al. (2018) functionalized carboxymethyl chitosan with HPEI to remove Hg(II) from wastewater. The concentration of Hg(II) ions was reduced from 798.1 to 0.02 mg/L, which was well below the permissible limit (0.05 mg/L) set for industrial wastewater in China.[24] This was due to the large number of $-NH_2$, which acted as metal binding groups toward Hg(II) ions. Humin, a byproduct generated in the preparation of humic acid, was modified with HPEI for the remediation of Cd(II) from water. Humin can be applied as an adsorbent for the remediation of heavy metals, but its direct application is limited by its low adsorption capacity. To overcome this drawback, humin was functionalized with HPEI to enhance the available adsorption sites, thereby improving efficiency. The X-ray photoelectron spectroscopy (XPS) analysis show that the N atoms from HPEI played an important role in the adsorption of Cd(II), and this resulted in an adsorption capacity of 11.975 mg/g. The performance was almost 5 times than that of unfunctionalized humin.[25] The removal of Ag^+ ions and the recovery of Ag^0 using polyethylenimine-modified potassium tungsten oxide ($K_2W_4O_{13}$) as an adsorbent were investigated.[26] Potassium tungsten oxide can act as an adsorbent as well as a reducing agent. The incorporation of PEI improved the removal efficiency

https://doi.org/10.1021/acsomega.3c06491
ACS Omega 2024, 9, 8954−8972

Scheme 1. Reaction Scheme of (a) Aldehyde Group of Glutaraldehyde and the −OH on the CFA Forming Acetal, (b) Possible Cross-linking through the Reaction of the Aldehyde Group with the N Atom on the HPEI Resulting in the Formation of (c) CFA−HPEI Adsorbent

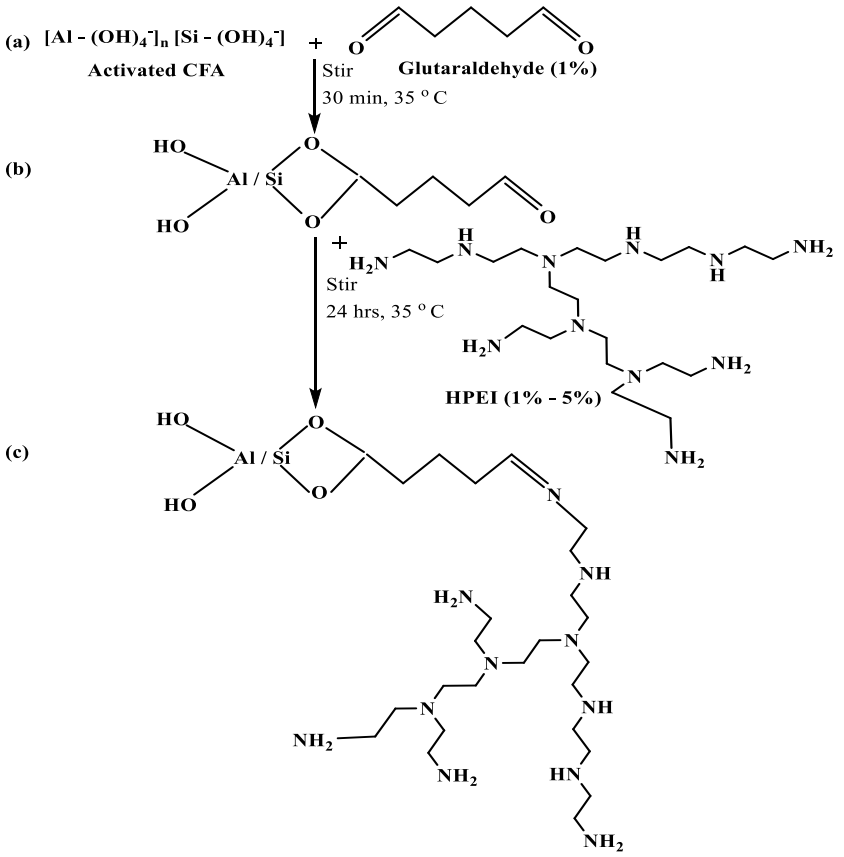

of the adsorbent and its reduction properties. The significant improvement in efficiency is a result of the interaction between N atoms of the PEI and Ag^+ ions, and electron transfer occurs resulting in the reduction of Ag^+ ions to Ag^0.[26]

In this study, CFA was modified with HPEI for the removal of Cr(VI) from water. The modification was made possible by first activating the CFA to introduce the −OH groups on the material, followed by adding glutaraldehyde, which is a cross-linker through the reaction of the aldehyde group on the glutaraldehyde and the −OH group on the CFA. The addition of HPEI resulted in the reaction between the aldehyde functional group and the N atom from the HPEI molecule. After the application of the CFA−HPEI adsorbent to remove Cr(VI), chromium is reduced to less toxic Cr(III) by electrons from HPEI (reducing agent causes transfer of electrons from the lone pair of electrons on the N atoms of the HPEI). The reduction step displays a novel method that alleviates Cr(VI) in wastewater. Another innovative aspect of this work is that the adsorbent is reused as the photocatalyst to degrade the methylene blue (MB) dye in wastewater due to the presence of Cr(III), which is safe for environment. The CFA−HPEI works as the multifunctional adsorbent and a photocatalyst which has a high potential for water treatment in municipalities and wastewater treatment plant.

2. REAGENTS AND METHODS

2.1. Reagents. Ammonium nitrate (NH_4NO_3, ≥99%), glutaraldehyde (Grade II, 25% in H_2O), hydrochloric acid (HCl, 32 wt %), HPEI (MW 25,000 g/mol), magnesium sulfate heptahydrate ($MgSO_4{\cdot}7H_2O$, ≥99%), and methanol [CH_3−OH, high-performance liquid chromatography (LC) 99.9%] were all purchased from Sigma-Aldrich, South Africa). Potassium dichromate ($K_2Cr_2O_7$, ≥99%), sodium chloride (NaCl, ≥99%) and sodium hydroxide (NaOH, ≥99%) were all purchased from Merck, South Africa, while MB ($C_{16}H_{18}ClN_3S{\cdot}xH_2O$, AR) was purchased from Reflecta Laboratory Supplies. CFA was collected from a coal-fired power station in South Africa. All working solutions were prepared using deionized water.

2.2. Pretreatment, Activation, and Functionalization of CFA. The pretreatment of the CFA was performed according to the method reported by Chen et al. (2018) through washing with deionized water (1:6 m/v) while stirring at room temperature for 1 h.[27] The resulting slurry was filtered off and dried in a 105 °C oven at for 12 h. The dried solid was ground into a fine powder and characterized. The CFA was mixed with NaOH (5:8 w/w) and calcined at a temperature of 300 °C for 3 h. The fused mass was allowed to cool to room temperature, ground, and washed with deionized water. The resulting slurry was filtered and dried for 12 h in an oven at 105 °C.[28] CFA (20 g) was dispersed in methanol. The glutaraldehyde solution (1% w/v) was added dropwise to the mixture. The mixture was left to stand for 30 min under continuous stirring. The HPEI solution in methanol (1−5% w/v) was added. The mixture was stirred at 180 rpm for 24 h at 35 °C for cross-linking.[29] CFA mainly contains Al_2O_3 and SiO_2, which were converted to Al−$(OH)_4^-$ and Si−$(OH)_4^-$ by treatment with NaOH to introduce the −OH groups on the surface. The functionalization of the

https://doi.org/10.1021/acsomega.3c06491
ACS Omega 2024, 9, 8954−8972

activated CFA was performed adopting the methods as outlined by Troung et al. (2020) and Xiao et al. (2010).[20,30] The addition of glutaraldehyde resulted in a reaction between the aldehyde group and the −OH on the CFA forming hemiacetal, successively with another −OH resulting in a full acetal. The HPEI added reacted with the aldehyde functional group on the glutaraldehyde and the N atom on the HPEI as shown in Scheme 1.

2.3. Characterization. X-ray fluorescence (XRF) spectroscopy was used to determine the elemental composition of raw CFA. The sample was poured into an aluminum cup and pressed to form a pellet under high pressure (20 tons) for 60 s. MagiX PRO XRF spectrophotometer (Malvern Panalytical, United Kingdom) was used for analysis, and it was operated at 40 kV and 40 mA. The crystallinity measurements of the CFA were carried out using an X'Pert PRO X-ray Diffractometer (Malvern Panalytical, United Kingdom) using Ni-filtered Cu-Kα (λ = 0.1540 nm) radiation equipped with an X'Celerator detector. The generator was operated at 40 kV and 40 mA. The samples were scanned over 2θ degree angle of 4−80°. The surface chemical state of the adsorbents was determined using an ESCALAB 250Xi X-ray Photoelectron Spectrometer (Thermo Fisher Scientific, USA) equipped with a monochromatic Al kα X-ray source (1486.6 eV). The functional groups present were determined using a Fourier transform infrared (FTIR) spectrometer (PerkinElmer, Germany). Samples were combined with KBr at a dilution ratio of 1:99 to make pellets before FTIR analysis. The surface morphology of the materials was determined using a TESCAN VEGA3 scanning electron microscopy−energy-dispersive X-ray spectrometry (Czech Republic). The high voltage was operated at 20 kV. The surface area measurements were determined using Micromeritics ASAP 2460 (USA) Brunauer−Emmett−Teller (BET) surface area measurements by N_2 adsorption at −196 °C. Samples were degassed at 90 °C for 9 h before analysis. The zeta potential measurements were conducted using a Malvern Panalytical Zetasizer Nano-ZS (United Kingdom). The samples were dispersed in deionized water prior to analysis. An elemental analyzer (FLASH 2000 series, Thermo Fischer Scientific, USA) was utilized to determine the elemental composition of the samples. The optical properties of the adsorbents were determined using a Shimadzu UV-2450 spectrometer in the diffuse reflectance spectroscopy (DRS) mode. The band gaps were calculated from the DRS data. The photodegradation products of MB were analyzed by LC−mass spectrometry (MS). A Waters Synapt G1 HDMS mass spectrometer with Waters Acquity UPLC (USA) was used.

2.4. Batch Experiments. 2.83 g of potassium dichromate ($K_2Cr_2O_7$) was dissolved in deionized water to make up a 1000 mg/L stock solution. The adsorption experiments were conducted in a thermostatic shaker set to 160 rpm. All experiments were conducted in triplicate and results reported with error bars. The effect of adsorbent dosage and pH was investigated to optimize the adsorption behavior (see the Supporting Information). Varying amounts (10−70 mg) of CFA and CFA−HPEI adsorbents (1−5%) were suspended in 20 mL of Cr(VI) solution (20 ppm) at 25 °C. A 20 mL aliquot of the 1000 ppm stock solution was accurately pipetted into a volumetric flask. The actual concentration was determined using a UV−vis spectrophotometer through the 1,5-diphenylcarbazide method.

The effect of pH was studied by varying the solution pH from 2 to 11. This was achieved by adjusting the solutions with either 0.1 M HCl or 0.1 M NaOH solution. The Cr(VI) concentrations of the solutions were measured with a UV−visible spectrophotometer (Shimadzu UV-1800) at 540 nm using the 1,5-diphenylcarbazide method.[31] The removal percentage of Cr(VI) was calculated using eq 1.

$$\%\ \text{removal} = \left(\frac{C_0 - C_e}{C_0}\right) \times 100 \tag{1}$$

where C_0 and C_e (mg/L) represent the initial and equilibrium concentrations of Cr(VI), respectively.[32]

The amount adsorbed at time t expressed as q_t was calculated using eq 2.

$$q_t = \left(\frac{C_0 - C_t}{m}\right)V \tag{2}$$

where q_t (mg/g) is the amount of Cr(VI) adsorbed per unit mass of the adsorbent at time t, C_t(mg/L) is the Cr(VI) concentration at time, m(g) is the mass of the adsorbent, and V(L) is the volume of Cr(VI) solution. The adsorption capacity of the adsorbent at equilibrium, q_e (mg/g), was calculated using eq 3.[32]

$$q_e = \left(\frac{C_0 - C_e}{m}\right)V \tag{3}$$

2.5. Adsorption Kinetics. Based on the results obtained during optimization when studying the effect of pH and adsorbent dosage, the 3% loaded CFA−HPEI adsorbent was used to investigate the kinetics associated with the adsorption of Cr(V1). Adsorption kinetics is important in determining the rate-determining step in an adsorption process in order to provide an understanding into the design and modeling of an adsorption-based water treatment process. The adsorption kinetics data was evaluated using pseudo-first-order and pseudo-second-order kinetic models. The linear eqs 4 and 5 of the two models are displayed below

$$\text{pseudo-first-order kinetic model: } \ln(q_e - q_t) = \ln q_e - k_1 t \tag{4}$$

$$\text{pseudo-second-order kinetic model: } \frac{t}{q_t} = \frac{1}{k_2 q_e^2} + \frac{t}{q_e} \tag{5}$$

where t(min) is time and k_1 and k_2 are the rate constants (min^{-1}).[33]

The rate-limiting step for the uptake of Cr(VI) was determined using the intraparticle diffusion model in eq 6.

$$q_t = k_i t^{0.5} + C \tag{6}$$

where k_i (mg/g min$^{0.5}$) represents intraparticle diffusion rate constant and C is the intercept related to boundary layer thickness.[34]

2.6. Adsorption Isotherms. The adsorption isotherms were performed at temperatures of 25, 35, and 45 °C. The concentration ranged from 20 to 500 mg/L at pH 2.0. The equilibrium adsorption data was evaluated using Langmuir and Freundlich adsorption isotherm models presented by eqs 7 and 8, respectively

$$\frac{C_e}{q_e} = \frac{1}{q_m b} + \frac{C_e}{q_m} \tag{7}$$

https://doi.org/10.1021/acsomega.3c06491
ACS Omega 2024, 9, 8954−8972

where q_m (mg/g) represents the maximum adsorption capacity, b (L/mg) is the adsorption free energy, and C_e (mg/L) is the adsorbate concentration at equilibrium

$$\log q_e = \log K_F + \frac{1}{n}\log C_e \quad (8)$$

where K_F ($mg^{1-1/n}\ L^{1/n}\ g^{-1}$) is the Freundlich constants related to adsorption capacity and n (dimensionless parameter) is the adsorption intensity.[35] The thermodynamics parameters for the adsorption of Cr(VI) by the CFA−HPEI (3%) adsorbent such as changes in enthalpy (ΔH^0), entropy (ΔS^0), and standard Gibbs free energy (ΔG^0) were calculated using the following equations

$$K_c = m\frac{q_e}{C_e} \quad (9)$$

$$\ln K_c = \frac{\Delta S^0}{R} - \frac{\Delta H^0}{RT} \quad (10)$$

$$\Delta G^0 = -RT \ln K_c \quad (11)$$

where K_c is the adsorption affinity at the lowest experimental Cr(VI) concentration, R denotes ideal gas constant (J/mol/K), and T is the absolute temperature (K).[36]

2.7. Interference Studies. The effect of other coexisting ions like Cl^-, NO_3^-, SO_4^{2-}, Cu^{2+}, Fe^{2+}, and Zn^{2+} on the adsorption of Cr(VI) was also investigated. The experiments were performed with 20 mL of 20 mg/L Cr(VI) solutions containing 10, 20, 30, 40, or 50 mg/L of Cl^-, NO_3^-, and SO_4^{2-} and 30 mg of the adsorbent. All solutions were adjusted to pH 2.0. The adsorption was allowed to reach equilibrium after which the residual Cr(VI) was determined. Table S1 illustrates the preparation of the solutions.

2.8. Reusability Studies. 100 mg of the CFA−HPEI-Cr was transferred into a cylindrical glass reactor containing 500 mL solution of 5 mg/L MB solution. The mixture was allowed to equilibrate for 30 min in the dark before being irradiated with a visible lamp (250 HW). During irradiation, the mixture was agitated vigorously. At regular interval times, 10 mL aliquots were taken, filtered using 0.45 μm syringe filters, and analyzed using a UV−visible spectrophotometer to determine the residual MB. The maximum absorbance was obtained at a wavelength of 665 nm. The photocatalytic degradation was calculated using eq 12.

$$\%\ \text{degradation} = \left(\frac{C_0 - C_t}{C_0}\right) \times 100 \quad (12)$$

The kinetics rate of degradation of MB by CFA−HPEI (3%) adsorbent and Cr-loaded CFA−HPEI (3%) adsorbent was determined using the pseudo-first-order eq 13.

$$\ln(C_t/C_0) = -Kt \quad (13)$$

where C_0 (mg/L) is the initial concentration at t_0, C_t (mg/L) represents MB concentration during visible light irradiation at different time intervals t (min), and the rate constant (K) is the slope of the graph.[37]

2.9. Determination of Degradation Products Using LC−MS. The photodegradation products of MB were analyzed by LC−MS. A Waters Synapt G1 HDMS mass spectrometer with Waters Acquity UPLC (USA) was used. The LC was equipped with a Waters Acquity T3 C18 column (150 × 2.1 mm) operated at 60 °C. The MS was equipped with an electrospray ionization source operated in positive mode with a capillary voltage of 2.5 kV, cone voltage of 30 V, drying gas flow rate of 7.5 L/min, and an operating pressure of 8500 psi. The eluents used were A (water with 0.1% formic acid) and B (acetonitrile with 0.1% formic acid) set at linear gradient flow from 100% A to 2% A in 6 min at a flow rate of 0.4 mL/min with a sample injection volume of 10 μL.

2.10. Data Analysis. All experiments were reported as the mean of three replicates. The kinetics data and equilibrium isotherm models were evaluated using Origin Pro 8.5. The X-ray diffraction (XRD) data were processed with HighScore Plus 4.9, while XPS data were processed with Thermo Avantage 5.9.

3. RESULTS AND DISCUSSION

3.1. Characterization of CFA and CFA−HPEI (1−5%) Adsorbents. *3.1.1. XRF Analysis.* The CFA was primarily composed of SiO_2 (46%), Al_2O_3 (31%), CaO (5.9%), and Fe_2O_3 (2.4%). As depicted in Table 1, there were also small amounts of

Table 1. Chemical Composition of CFA

component	%
SiO_2	46
Al_2O_3	31
CaO	5.9
Fe_2O_3	2.4
TiO_2	1.5
MgO	1.4
P_2O_5	1.0
K_2O	0.72
Na_2O	0.60
LOI	2.35

TiO_2, MgO, P_2O_5, K_2O, and Na_2O present. Similar results were obtained for CFA collected from other power stations in South Africa.[38−40] The elemental analysis results show that this CFA is class F fly ash as defined by the American Society for Testing Materials Standard C618.[41]

3.1.2. XRD Analysis. Figure 1 depicts the XRD patterns for CFA, CFA−NaOH, and CFA−HPEI (1−5%) adsorbents. The results showed that CFA consists mainly of quartz (SiO_2) and mullite ($Al_6Si_2O_{13}$) as confirmed by ICSD 01-070-3755 and

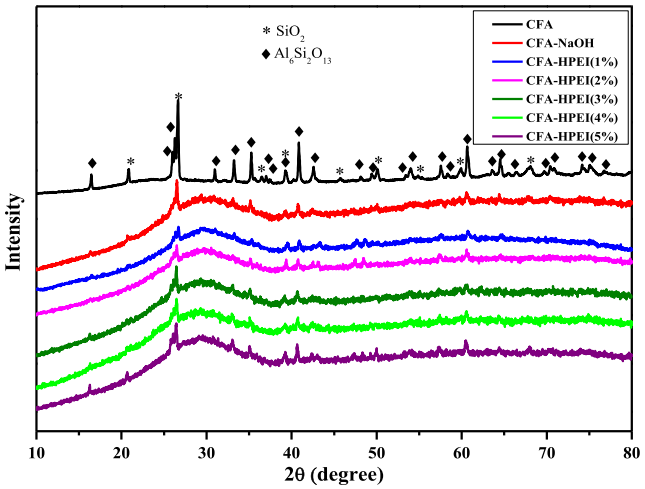

Figure 1. XRD patterns for CFA, CFA−NaOH, and CFA−HPEI (1−5%) adsorbents.

https://doi.org/10.1021/acsomega.3c06491
ACS Omega 2024, 9, 8954−8972

ICSD 01-083-1881, respectively. These results correspond with recent studies reported on the analysis of fly ash in South Africa.[42,43] As reported, the activation of CFA with NaOH resulted in the destruction of the crystalline structure of CFA as shown by the sharp decrease in the intensity of the diffraction peaks of CFA, with no new crystalline phases formed.[28,44] While the HPEI loading onto the activated CFA−NaOH was varied from 1 to 5%, the diffraction patterns obtained show that the variation in HPEI did not result in differences in the crystal structure of the activated CFA. They all showed low-intensity peaks associated with the presence of quartz and mullite.

3.1.3. SEM−EDS Analysis. The surface morphology of CFA, CFA−NaOH, and CFA−HPEI adsorbents was analyzed using SEM−EDS. The CFA particles were spherical in shape with varying particle sizes, with an average particle size of 4.05 μm, as shown in Figure 2. The surface morphology of CFA particles

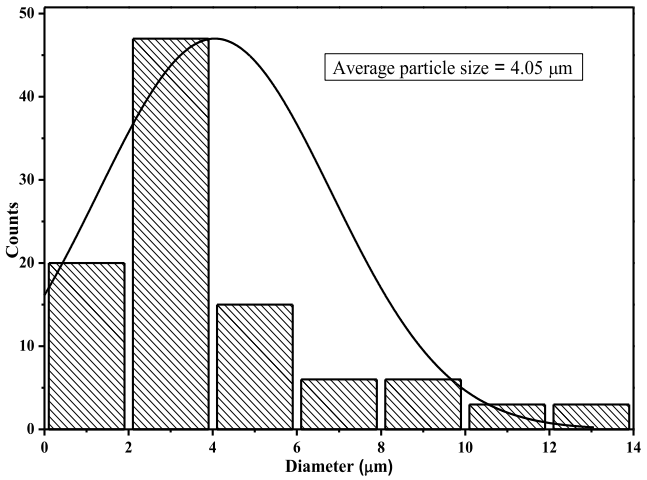

Figure 2. Particle size distribution for CFA.

show relatively leathery surfaces, as depicted in Figure 3a.[45,46] The energy-dispersive spectrometry (EDS) spectrum (Figure 3h) reveals that the CFA is primarily composed of O, Al, Si, Ca, and Fe. This data corresponds with the data obtained from the EDS analysis and is also similar to other studies reported on South African CFA.[47,48] The alkali-activated CFA (Figure 3b) shows a change in the morphology of the CFA particles: the smooth spherical structure of CFA particles changed to irregular agglomerates with rough surfaces. The EDS (Figure 3i) displays the presence of Na that was attached to the surface of CFA during the activation process. After the functionalization of CFA−NaOH with HPEI, the EDS spectra for CFA−HPEI (1−5%) adsorbents (Figure 3j−n) show a significant increase in the quantity of carbon, which is attributed to the presence HPEI. An increase in HPEI loading on the CFA did not result in any significant change in the surface morphology of the CFA−HPEI (1−5%) adsorbents, as shown in Figure 3c−g.

3.1.4. FTIR Analysis. FTIR analysis was carried out to identify the functional groups present in CFA, CFA−NaOH, and CFA−HPEI (1−5%) adsorbents and to monitor the change in intensity or shift in peak positions. As shown in Figure 4, the CFA shows a peak at 1096 and 551 cm^{-1}, which depicts the presence of Si−O−Si symmetric and asymmetric stretch vibrations and Fe−O vibrations, respectively. CFA−NaOH shows a broad peak at 3440 cm^{-1} (Si−OH) and a peak at 1651 cm^{-1} due to the presence of −OH vibrations.[49] The HPEI-functionalized CFA shows a change in the shape and intensity of the peaks due to the −OH vibrations (3440 cm^{-1}) and Si−O−Si vibrations (992 cm^{-1}) caused by the interaction of CFA−NaOH and HPEI. There are also new peaks at 2847 and 2971 cm^{-1} because of the presence of sp^3-hybridized carbons in the HPEI chain. The additional peak at 1482 cm^{-1} is attributed to the presence of C−H bending vibrations, confirming the successful functionalization of CFA.[49,50] In addition, the peak at 1651 cm^{-1}, attributed to C═N stretch vibrations is enhanced, which further confirms the successful incorporation of HPEI onto CFA.[51]

Table 2. BET Surface Areas of CFA, CFA−NaOH, and CFA−HPEI (1−5%) Adsorbents

	Surface area (m^2/g)
CFA	1.25
CFA−NaOH	17.9
CFA−HPEI (1%)	15.3
CFA−HPEI (2%)	15.0
CFA−HPEI (3%)	16.2
CFA−HPEI (4%)	16.6
CFA−HPEI (5%)	16.1

3.1.5. BET Analysis. The specific surface area of raw CFA was found to be 1.24 m^2/g. The activation of CFA using NaOH resulted in a significant increase in specific surface area to 17.9 m^2/g (Table 2). Similar results were reported by Meng et al. (2020) and Woolard et al. (2000) after treating CFA with NaOH. In both studies, the specific surface area was found to increase from 1.05 to 62.66 m^2/g[44] and from 1.58 to 23.6 m^2/g.[52] After functionalization of the activated CFA with HPEI, the specific surface area decreased to 15.3 m^2/g for the CFA−HPEI (1%), with an increase from 15.0 to 16.6 m^2/g as the CFA−HPEI loading increases (Table 2). The incorporation of HPEI in the CFA resulted in a decrease in the specific surface area, which is due to the blockage of pores by the HPEI.[49] There is no significant difference in BET surface area for the 3-, 4-, and 5%-HPEI-loaded adsorbents, which suggests optimum loading. The CFA, CFA−NaOH, and CFA−HPEI (1−5%) adsorbents exhibited features of non porous or macroporous adsorbents with reversible BET type 2 isotherm (Figure 5).

3.1.6. Elemental Analyses. The elemental analyses of the raw CFA and the functionalized CFA were performed, and the results are given in Table 3. The raw CFA had an average of 3.86 and 0% of carbon and nitrogen, respectively. The functionalization of CFA with HPEI resulted in an increase in both carbon and nitrogen contents: the CFA−HPEI (1%) adsorbent had an average of 4.48 and 0.83% of carbon and nitrogen, respectively. An increase in HPEI loading to 2 and 3% resulted in an increase in the percentages of both carbon and nitrogen. Further increase in HPEI loading to 4 and 5% resulted in a decrease in carbon and nitrogen content: an average of 5.38% of carbon and 1.69% of nitrogen were obtained from the CFA−HPEI (4%) adsorbent, while the CFA−HPEI (5%) adsorbent had an average of 3.44 and 0.75% of carbon and nitrogen, respectively. The decrease in carbon and nitrogen content was caused by the hindrance effect of the −OH groups on the CFA by the bulky HPEI molecules that might have occurred as the percentage of HPEI increased. The presence of nitrogen in the functionalized CFA confirms the successful incorporation of HPEI onto CFA.[29,53]

3.2. Application of CFA−HPEI Adsorbents for the Removal of Hexavalent Chromium (Cr(VI)). *3.2.1. Effect of Adsorbent Dosage on the Uptake of Cr(VI).* Adsorbent dosage is an important factor in adsorption studies as it influences the

https://doi.org/10.1021/acsomega.3c06491
ACS Omega 2024, 9, 8954−8972

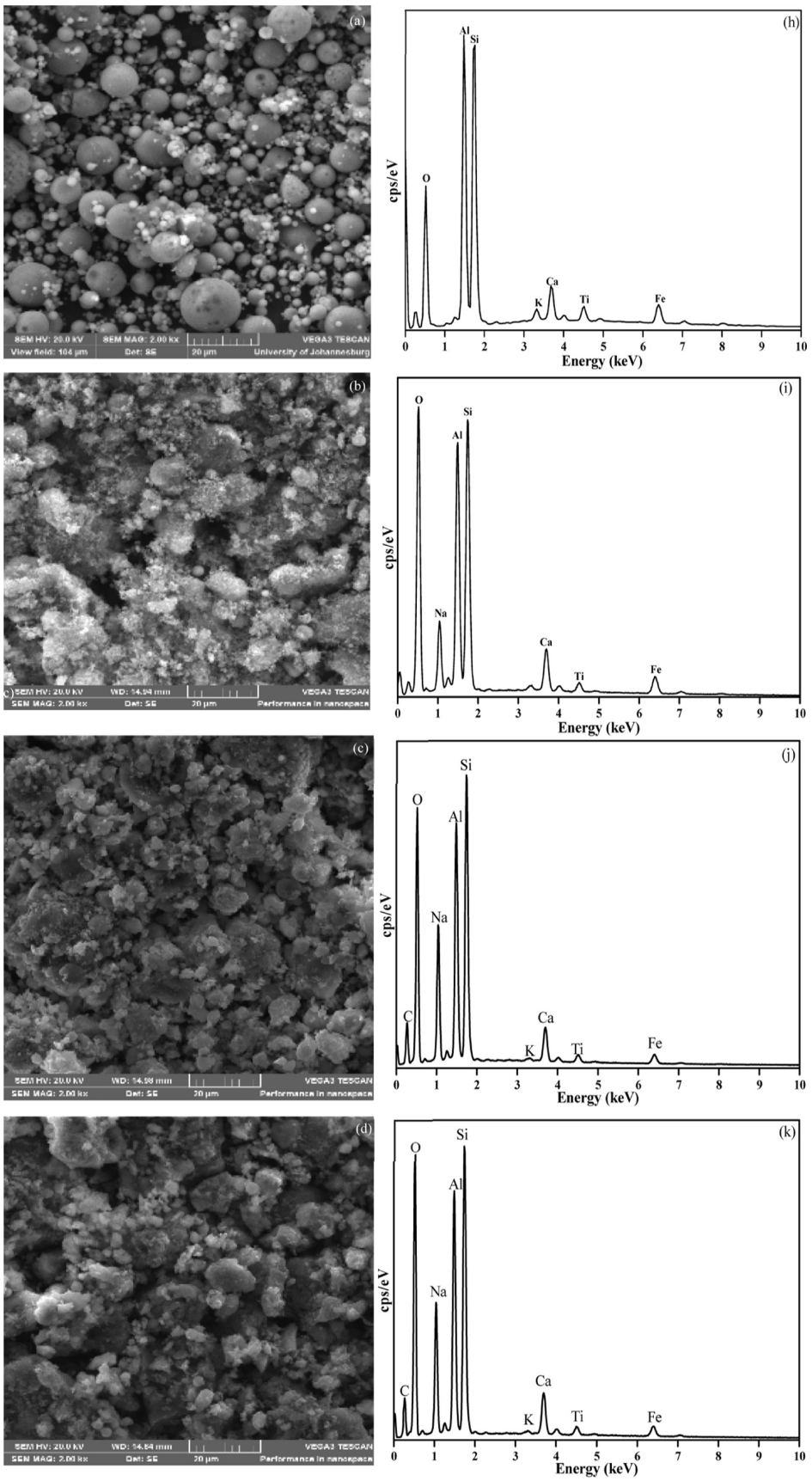

Figure 3. continued

https://doi.org/10.1021/acsomega.3c06491
ACS Omega 2024, 9, 8954−8972

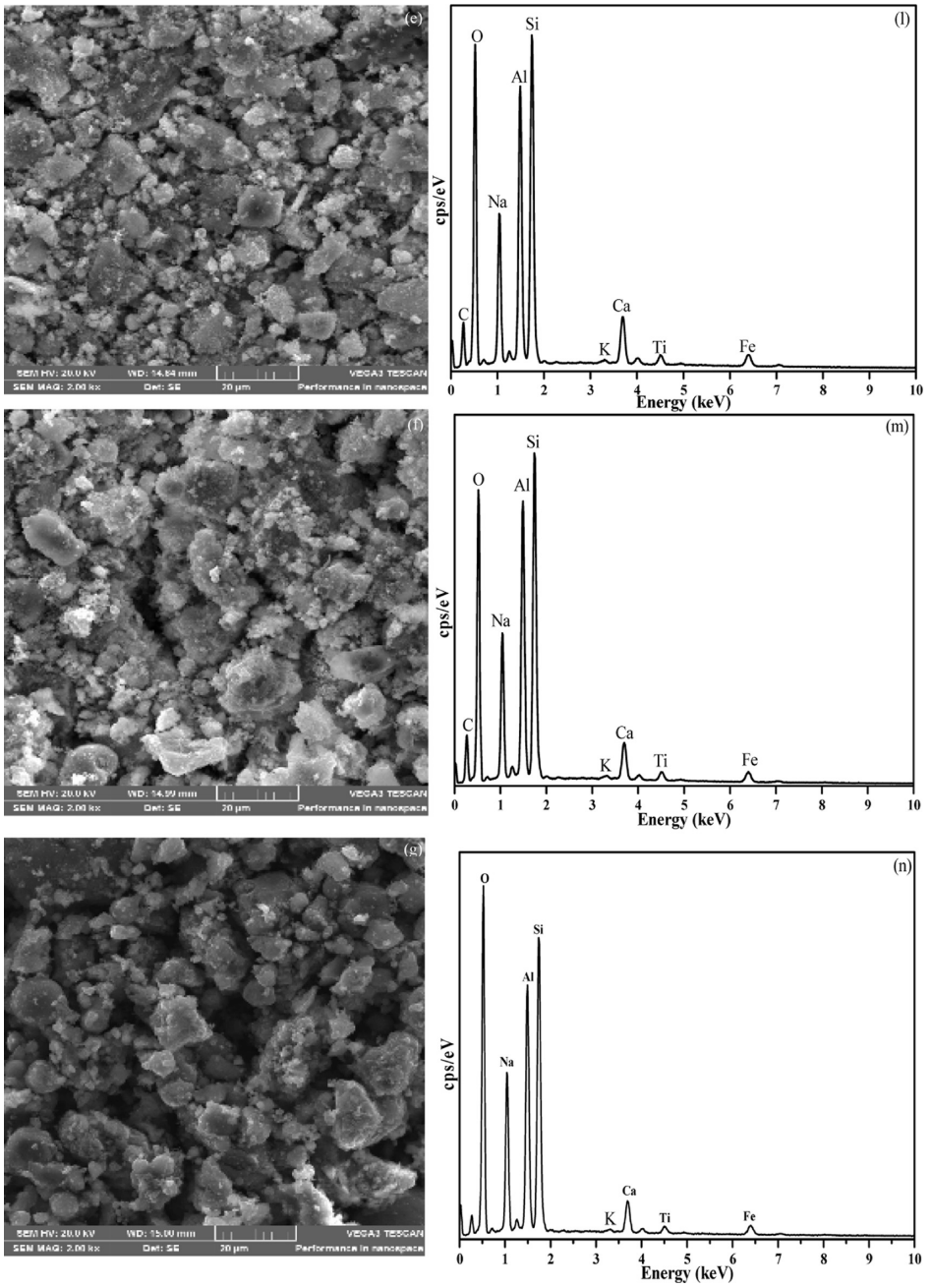

Figure 3. SEM micrographs for (a) CFA, (b) CFA−NaOH, (c−g) CFA−HPEI (1−5%) adsorbents, and EDS spectra for (h) CFA, (i) CFA−NaOH, and (j−n) CFA−HPEI (1−5%) adsorbents.

Table 3. Elemental Analyses Results of CFA and CFA−HPEI (1−5%) Adsorbents

	CFA	CFA−HPEI (1%)	CFA−HPEI (2%)	CFA−HPEI (3%)	CFA−HPEI (4%)	CFA−HPEI (5%)
C	3.87	4.48	5.10	6.93	5.38	3.44
H	0.37	2.09	2.17	3.57	2.24	1.92
N		0.83	1.58	1.86	1.69	0.75

adsorption capacity of an adsorbent at a specific initial concentration.[54] The adsorbent dosage ranged from 0.5 to 3.5 g/L (Figure 6). Raw CFA showed a low percentage removal of Cr(VI) with a maximum removal of 5.5% for 3.0 g/L adsorbent dosage. The maximum removal percentage was obtained from the CFA−HPEI (3%) and CFA−HPEI (4%) adsorbents with 98% removal obtained with adsorbent dosages of 1.5 g/L.

3.2.2. Effect of pH. pH is a critical factor for the adsorption of Cr(VI) because it affects the surface charge of the adsorbent and the Cr ionic speciation.[55] The pH was varied from pH 2 to 11, as depicted in Figure 7. The maximum Cr(VI) removal was obtained at pH 2 for the CFA−HPEI (1−5%) adsorbent and at pH 3 for the CFA. The adsorbents showed removal percentages between 65 and 95%, while the raw CFA displayed a low removal percentage of about 10%. In acidic medium (pH 2−6),

https://doi.org/10.1021/acsomega.3c06491
ACS Omega 2024, 9, 8954−8972

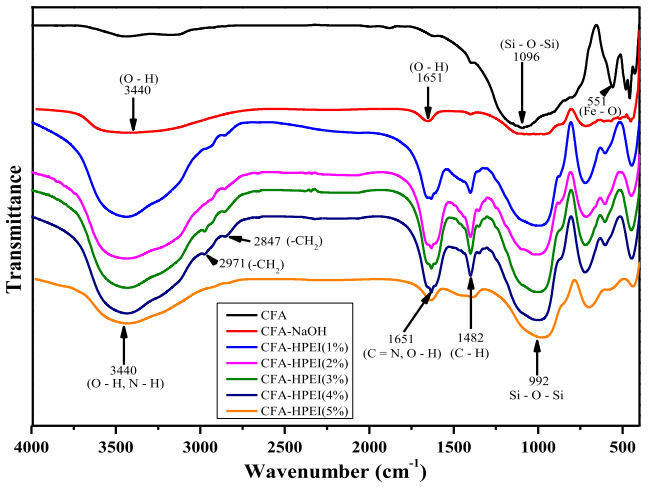

Figure 4. FTIR spectra of CFA, CFA−NaOH, and CFA−HPEI (1−5%) adsorbents.

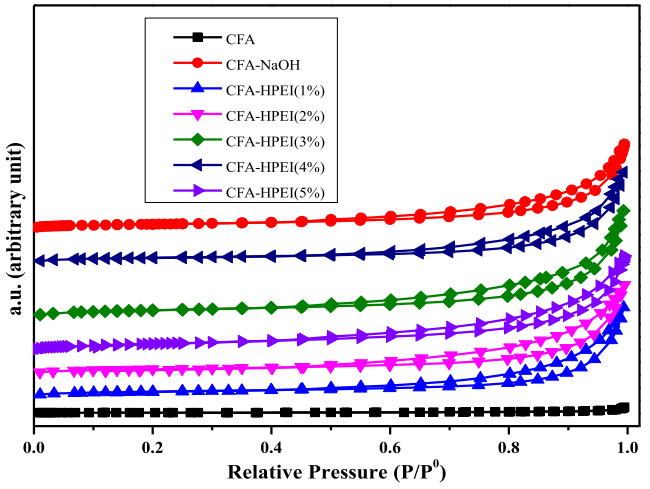

Figure 5. N_2 adsorption−desorption isotherms of CFA, CFA−NaOH, and CFA−HPEI (1−5%) adsorbents.

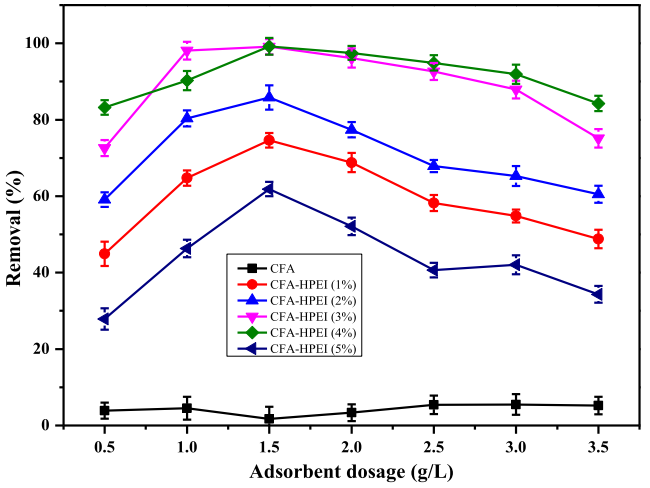

Figure 6. Effect of adsorbent dosage on the removal of Cr(VI) by CFA and CFA−HPEI (1−5%) adsorbents.

Cr(VI) exists as dichromate ($Cr_2O_7^{2-}$) and bichromate ($HCrO_4^-$) ions, which are major components in solution, while chromate (CrO_4^{2-}) ions dominate at pH above 6. Thus, the ions can be adsorbed on the positively charged surface through electrostatic attraction as shown by the zeta potential analysis in Figure 8.[56,57]

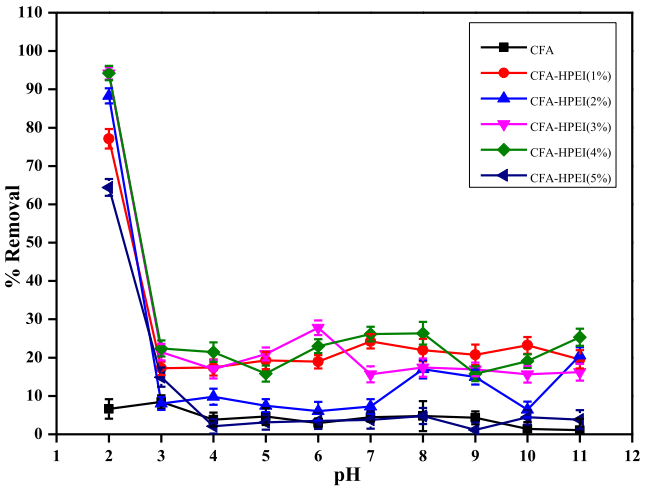

Figure 7. Effect of pH on the removal of Cr(VI) by CFA and CFA−HPEI (1−5%) adsorbents.

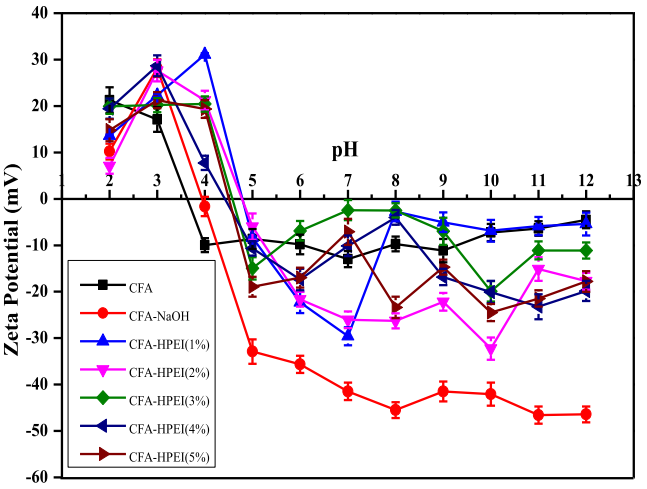

Figure 8. Zeta potential of CFA, CFA−NaOH, and CFA−HPEI (1%−5%) adsorbents.

The point of zero charge for CFA was 3.62, indicating that the adsorbent carried a positive charge below pH 3.6 and a negative charge above pH 3.6, with the zeta potential decreasing from +20 to −10 mV as the pH was increased from 2 to 12. The functionalization of CFA with HPEI resulted in the point of zero charge slightly increasing to 4.8, 4.78, 4.6, 4.40, and 4.5 for CFA−HPEI (1−5%) adsorbents. This showed that HPEI functionalization resulted in an increase in the zero point of charge of the adsorbent because of the protonation of the amine groups on HPEI.[58,59] Additionally, in acidic medium, the NH_2 groups in HPEI are protonated and form NH_3^+ which will attract the opposite charge on the dominating negatively charged Cr(VI) species, resulting in the uptake being higher at lower pH values. As the pH was increased, the removal percentage decreased due to less protonation of the NH_2 groups and also due to competition between the negatively charged Cr(VI) species and OH^- groups.[60]

3.2.3. Adsorption Kinetics. As depicted in Figure 9a, the influence of contact time on the removal of Cr(VI) by CFA−HPEI (3%) adsorbent was studied for three different initial

https://doi.org/10.1021/acsomega.3c06491
ACS Omega 2024, 9, 8954−8972

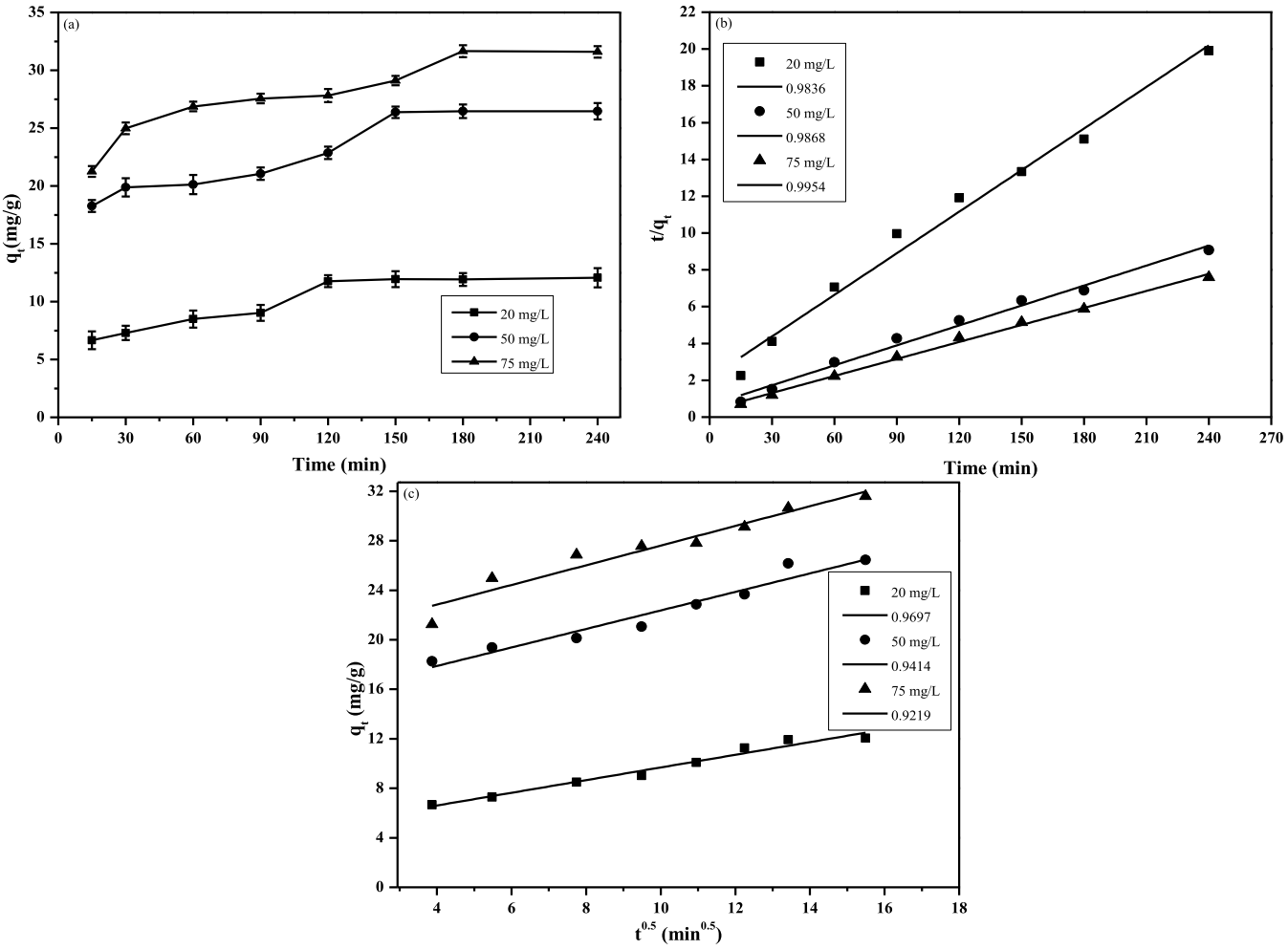

Figure 9. (a) Effect of contact time on the adsorption of Cr(VI) by CFA−HPEI (3%) adsorbent at initial concentrations of 20, 50, and 75 mg/L, (b) linear fit for pseudo-second-order kinetic model, and (c) intraparticle diffusion model for adsorption of Cr(VI) by CFA−HPEI (3%) adsorbent.

concentrations (20, 50, and 75 mg/L). An increase in the initial concentration resulted in an increase in the amount adsorbed, with equilibrium attained after 120, 150, and 180 min for the three different initial concentrations, respectively. Initially, Cr(VI) ions migrate to the boundary layer, then diffuse through to the adsorbent surface. Lastly, they diffuse onto the surface of the adsorbent material.[8] The 75 mg/L solution will require more contact time to reach equilibrium because of the higher number of Cr(VI) ions present. In addition, at the initial time of contact, there is a large number of vacant adsorption sites and also a high concentration gradient of Cr(VI) between the adsorbent and the bulk of the solution. As adsorption equilibrium was reached, the adsorption capacity remained unchanged because of the decrease in number of vacant sites available for adsorption and also a decrease in concentration gradient.[61,62] The kinetics data for pseudo-first-order and pseudo-second-order kinetic models are displayed in Table 4. As shown in Figure 9b, the pseudo-second-order kinetic model better defined the adsorption of Cr(VI) with R^2 values of 0.9836, 0.9868, and 0.9954 for Cr(VI) initial concentrations of 20, 50, and 75 mg/L, respectively. The q_e values obtained using the pseudo-second-order kinetic model were comparable to q_e experimental values. Adsorption kinetics are generally controlled by either external or intraparticle diffusion or both.[63] If a plot of q_t versus $t^{0.5}$ gives a linear relationship and the graph passes through the zero point, intraparticle diffusion is the rate-determining step.[64] Table 5 presents the correlation coefficients for the graphs displayed in Figure 9c. As the concentration is increased from 20 to 70 mg/L,

Table 4. Kinetic Parameters for the Adsorption of Cr(VI) by CFA−HPEI (3%) Adsorbents

	initial concentration (mg/L)205075		
	pseudo-first-order		
linear fit			
R^2	0.9448	0.9296	0.9505
k_1 (min^{-1})	0.01199	0.004721	0.006379
q_e (mg/g)	8.126	14.12	12.38
	pseudo-second-order		
linear fit			
R^2	0.9836	0.9868	0.9954
k_2 (g/mg/min)	0.002668	0.002025	0.002477
q_e (mg/g)	13.28	27.67	32.45

Table 5. Intraparticle Diffusion Model Parameters for the Adsorption of Cr(VI) by CFA−HPEI (3%) Adsorbent

	intraparticle diffusion		
initial concentration (mg/L)	K_i (mg/g min)	C (mg/g)	R^2
20	0.5120	4.562	0.9697
50	0.7478	14.89	0.9414
75	0.7951	19.66	0.9219

https://doi.org/10.1021/acsomega.3c06491
ACS Omega 2024, 9, 8954−8972

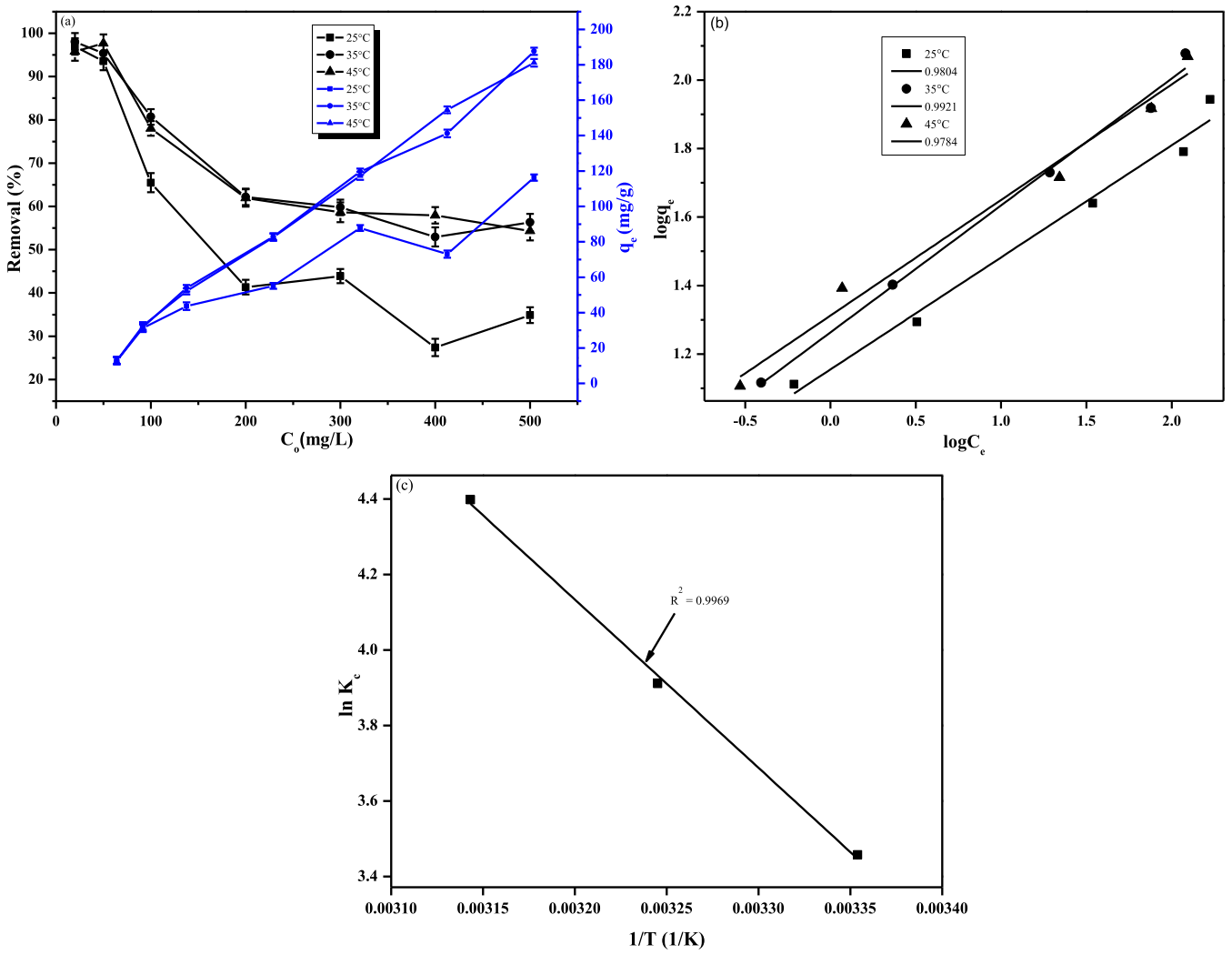

Figure 10. (a) Effect of temperature on the adsorption of Cr(VI) by CFA−HPEI (3%) adsorbent, (b) plot of log q_e (q_e, mg/g) against log C_e (C_e, mg/L), representing the linear Freundlich adsorption isotherm for Cr(VI) adsorption using CFA−HPEI (3%) adsorbent, and (c) graph to obtain the thermodynamic parameters for Cr(VI) adsorption using CFA−HPEI (3%) adsorbent.

the correlation coefficient (R^2) declines. Moreover, since the three graphs do not pass through the zero point this suggests that intraparticle diffusion is not the rate-determining step in the removal of Cr(VI) by the CFA−HPEI (3%) adsorbent.

3.2.4. Adsorption Isotherm Models. Adsorption isotherm experiments were performed to investigate the interaction between the adsorbent and adsorbate. The equilibrium adsorption data was studied at three different temperatures: 25, 35, and 45 °C. As shown in Figure 10a, the adsorption capacity increased with increasing temperature from 25 to 35 °C, indicating that the adsorption mechanism is endothermic. An increase in temperature to 45 °C did not result in any significant increase in adsorption capacity. The isotherm parameters obtained from the linear regression of the experimental data are summarized in Table 6. Higher correlation coefficient values (0.9804, 0.9921, and 0.9784) were obtained from the Freundlich adsorption isotherm as shown in Figure 10b, which suggests that this model fits the equilibrium adsorption data better than the Langmuir isotherm. The Freundlich isotherm model suggests that the surface of the adsorbent is heterogeneous.[65] The value of n indicates the favorability of the adsorption process. It is stated that an n in the range of 2−10 shows good adsorption characteristics.[66] In this study, the values of n obtained were 3.054, 2.698, and 2.962 for the three different temperatures, indicating that the adsorption process was favorable. The q_m values obtained were 58.58, 85.93, and 67.03 mg/g at the three different temperatures studied. The comparison of adsorption capacity of CFA−HPEI (3%) adsorbent with that of other low-cost adsorbents is tabulated

Table 6. Adsorption Isotherm Parameters for the Adsorption of Cr(VI) onto the CFA−HPEI (3%) Adsorbent

	temperature (°C)		
	25	35	45
Langmuir isotherm linear fit			
R^2	0.8512	0.9082	0.9058
b (L/mg)	15.52	12.87	14.25
q_m (mg/g)	80.52	118.6	117.9
Freundlich isotherm linear fit			
R^2	0.9804	0.9921	0.9784
N	3.054	2.698	2.962
K_F ($mg^{1-1/n}L^{1/n}g^{-1}$)	15.46	18.05	22.49
q_m (mg/g)	58.58	85.93	67.03

https://doi.org/10.1021/acsomega.3c06491
ACS Omega 2024, 9, 8954−8972

Table 7. Comparison of Maximum Adsorption Capacity of CFA−HPEI (3%) Adsorbent in Contrast with Other Low-Cost Adsorbent Materials Reported for the Adsorption of Cr(VI)

no	adsorbent	adsorption capacity (mg/g)	isotherms	references
1	alkali-modified CFA	5.976	Freundlich	68
2	polypyrrole-coated secondary fly ash−iron composites	119.33	Langmuir	69
3	natural akadama clay	4.290	Freundlich	54
4	polyethylenimine-impregnated activated carbon	114.0	Elovich and Langmuir	70
5	polyethylenimine−polyacrylamide−cellulose fibers	8.453	Langmuir	71
6	polyethylenimine-functionalized magnetic montmorillonite clay	62.89	Langmuir	72
7	polyethylenimine-modified activated-sludge-based adsorbent	86.96	Langmuir	73
8	CFA−HPEI (3%) adsorbent	85.93	Freundlich	this work

in Table 7. The data shows that the adsorbent performed much better than some of the adsorbents, while it was comparable in terms of amount adsorbed with other materials functionalized with PEI. A graph of ln K_c against $\frac{1}{T}$ is given in Figure 10c. ΔS^0 and ΔH^0 were calculated from the graph's intercept and slope, respectively. Table 8 shows that as temperature increased, the

Table 8. Thermodynamic Parameters for Cr(VI) Adsorption by CFA−HPEI (3%) Adsorbent

temperature (°C)	ΔG^0 (kJ/mol)	ΔS^0 (kJ/mol/K)	ΔH^0 (kJ/mol)
25	−8.57	0.1530	37.07
35	−10.1		
45	−11.6		

negative value for ΔG^0 increases. Together with a positive value for ΔH^0, this confirms that the adsorption process was spontaneous. A positive value of ΔS^0 indicates an increase in disorder at the solid−liquid interface.[67]

3.2.5. Interference Studies. Processes in the steel manufacturing industry produce wastewater containing Cr(VI) as well as other cations such as Cu^{2+}, Fe^{2+}, and Al^{3+} and anions such as Cl^-, NO_3^-, and SO_4^{2-}. The coexisting ions affect the binding force of the adsorbent and adsorbate during adsorption as it affects the potential and the width of the dual-layer around the adsorbent.[74,75] Coexisting ions such as Cl^-, NO_3^-, and SO_4^{2-} could exhibit a significant competitive effect, while cations could contribute to a synergetic adsorption effect on the adsorption of Cr(VI).[76] It is therefore critical to investigate the competitive effect of these coexisting ions on Cr(VI) remediation using CFA−HPEI (3%) adsorbent. As shown Figure 11, the concentration of the coexisting ions ranged from 10 to 50 mg/L. An increase in concentration of the coexisting ions had a slight effect on the adsorption of Cr(VI), with the 10 mg/L matrix resulting in 98% removal, while 50 mg/L resulted in 95% removal. The presence of positively charged ions is expected not to have an effect on the adsorption of Cr(VI) at pH 2 since Cr(VI) exists as a negatively charged ion ($HCrO_4$) while the adsorbent surface is positively charged, resulting in repulsion. On the contrary, the presence of an anion like SO_4^{2-} has the potential to decrease the uptake of $HCrO_4^-$ because of the comparable ionic radius of SO_4^{2-} and $HCrO_4^-$. The same ionic radius has comparable hydration energy,[77] hence the observed decrease as the concentration of coexisting ions increased.

3.2.6. Possible Mechanism for the Adsorption of Cr(VI) onto CFA−HPEI (3%) Adsorbent. The results obtained from varying the pH showed that the adsorption of Cr(VI) is pH-dependent with the maximum removal obtained at pH 2. At this pH, the NH_2 groups on CFA−HPEI get protonated, forming NH_3^+, which attracts the negatively charged Cr(VI) species. The

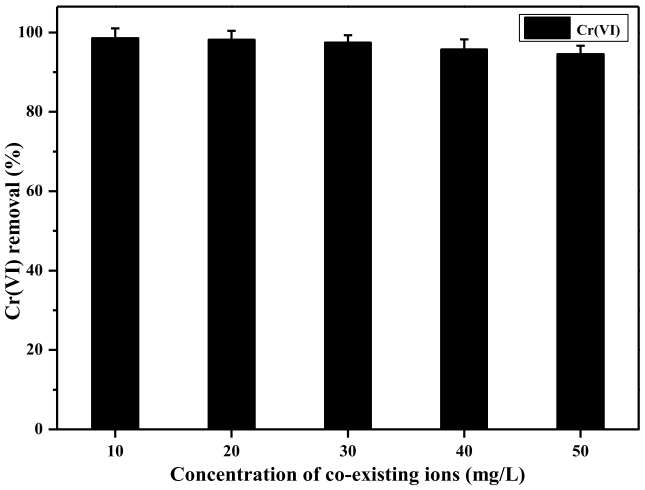

Figure 11. Effect of matrix on the adsorption of Cr(VI) using CFA−HPEI (3%) adsorbent.

Cr-loaded CFA−HPEI (3%) was also analyzed using BET, SEM−EDS, XPS, FTIR, and XRD. The adsorbent 's surface area decreased from 16.18 to 13.26 m^2/g. The decrease is due to Cr(VI) adsorbed on the surface of CFA−HPEI, as shown by the EDS elemental mapping analysis depicted in Figure 12.

The XPS was used to determine the mechanism responsible for the adsorption of Cr(VI) by CFA−HPEI (3%) adsorbent. As shown in Figure 13a, the spectrum shows energy bands due to Al 2p (73.7 eV), Si 2p (101.7 eV), Ca 2p (347.2 eV), Ti 2p (358.3 eV), O 1s (531.2 eV), Fe 2p (711.2 eV), Na 1s (1071.7 eV), and Mg 1s (1303.8 eV), all attributed to the CFA, and C 1s (285.7 eV) and N 1s (400 eV) attributed to HPEI. The deconvoluted spectrum of N 1s as shown in Figure 13b shows the energy bands at 399.9 and 401.3 eV attributed to −NH− and $-N^+=$, respectively, which are characteristic bands for HPEI. These results demonstrated that the amine groups from HPEI were successfully protonated, and Cr(VI) species which exist as negatively charged species in acidic medium could be effectively adsorbed on the protonated amino groups on surface of the CFA−HPEI (3%) adsorbent.[78] The adsorption of Cr(VI) onto the CFA−HPEI (3%) adsorbent is confirmed by the appearance of peaks observed at 577.3 and 587.9 eV due to Cr $2p^{3/2}$ and Cr $2p^{1/2}$, respectively, as shown in Figure 13c. Kera et al. reported similar results for Cr(VI) adsorption using polypyrrole/2,5-diaminesulfonic acid composite.[60] Furthermore, the deconvoluted spectrum of Cr 2p as shown in Figure 13d confirmed the presence of Cr(III) and Cr(VI) on the surface of the adsorbent with 77% of Cr(III), signifying reduction of the toxic Cr(VI) into less toxic Cr(III) which is less of a threat to the environment.[79−82] The HPEI acted as a reducing agent by

https://doi.org/10.1021/acsomega.3c06491
ACS Omega 2024, 9, 8954−8972

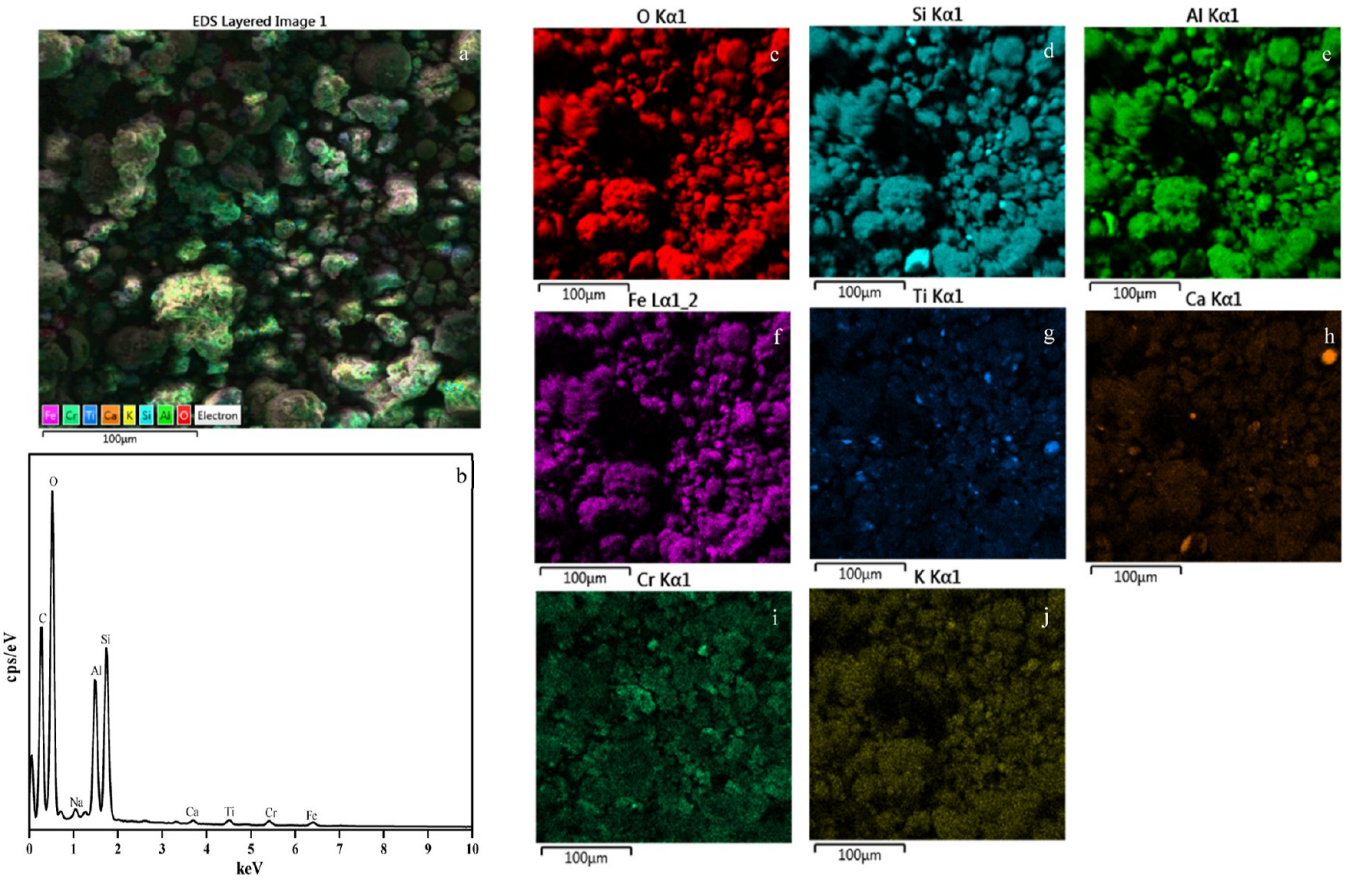

Figure 12. (a,c–j) EDS elemental mapping analysis of the Cr(VI)-loaded CFA–HPEI (3%) adsorbent and (b) EDS spectrum.

transferring electrons from the lone pair of electrons on the N atoms of the HPEI. This behavior was also observed by a study reported by Huang et al. (2019), where polyethylenimine-modified potassium tungsten oxide for the removal of Ag^+ and the recovery of Ag^0 was studied.[26] Also, the intensity of the N 1s (400 eV) peak decreased significantly after adsorption (Figure S1), implying that the N atom plays a role in the removal of Cr(VI).[83]

The FTIR spectra (Figure 14) show a shift in wavenumber of the peaks associated with O–H and N–H vibrations from 3440 to 3416 cm^{-1}. There is also a shift from 1655 to 1628 cm^{-1} for the peak related with O–H and N–H vibrations. The Si–O–Si peak has also shifted from 719 to 608 cm^{-1}. This behavior was expected because of the interaction between the functional groups on the surface of CFA–HPEI (3%) adsorbent and Cr(VI).[48] The XRD spectra in Figure 15 present the CFA–HPEI (3%) adsorbents before and after adsorption of Cr(VI). The peaks at 2θ degree angles of 20.93 and 29.59° associated with SiO_2 and $Al_6Si_2O_{13}$, respectively, are also observed on the diffraction pattern of the loaded adsorbent. Furthermore, no new peaks were observed in the FTIR and XRD spectra, implying that there were no changes in the structural integrity of the adsorbent after the removal process.

3.2.7. Optical Properties of the Adsorbents. The optical properties of CFA–HPEI (3%) adsorbent and Cr-loaded CFA–HPEI (3%) adsorbent were obtained by conducting UV–vis diffuse reflectance measurements. As shown in Figure 16a,b, the clean CFA–HPEI (3%) adsorbent exhibited a band gap of 3.52 eV, while the Cr-loaded CFA–HPEI (3%) adsorbent showed a slight decrease with a band gap of 3.40 eV, respectively. The decrease in band gap of the Cr-loaded CFA–HPEI (3%) adsorbent is due to the existence of Cr adsorbed on the surface of the CFA–HPEI (3%) adsorbent. Generally, a smaller band gap enables greater absorption of visible light by the material, while photocatalytic reactions with materials which exhibit larger band gaps result in less absorption of visible light, thus lowering the photocatalytic properties.[84] Due to its band gap value, the Cr-loaded CFA–HPEI (3%) adsorbent is therefore considered a better photocatalyst than the clean CFA–HPEI (3%) adsorbent.

3.2.8. Reusability Study of Cr-Loaded CFA–HPEI (3%) Adsorbent in the Photocatalytic Degradation of MB. The Cr-loaded CFA–HPEI (3%) adsorbent was studied as a photocatalyst to degrade MB. MB solution (5 ppm; 500 mL) was used as working solution together with 100 mg of the adsorbent. The reaction was monitored for 180 min for both CFA–HPEI (3%) adsorbent and Cr-loaded CFA–HPEI (3%) adsorbent. The maximum absorbance of MB was detected at a wavelength of 665 nm with the intensity decreasing as the irradiation time was increased, as depicted in Figure 17a,b. Figure 17c shows 93.7 and 98.9% MB removal efficiency by CFA–HPEI (3%) adsorbent and Cr-loaded CFA–HPEI (3%) adsorbent, respectively. As depicted in Figure 17c, about 32 and 40% MB removal efficiencies are observed during equilibration time, which suggests that adsorption may be occurring between MB and CFA–HPEI (3%) adsorbent. The adsorption process may be through electrostatic interactions between the negatively charged surface of the CFA–HPEI (3%) adsorbent as confirmed by zeta potential analysis (Figure 8) and the positive charge of MB, hydrogen bonding between amine groups of HPEI and the

https://doi.org/10.1021/acsomega.3c06491
ACS Omega 2024, 9, 8954–8972

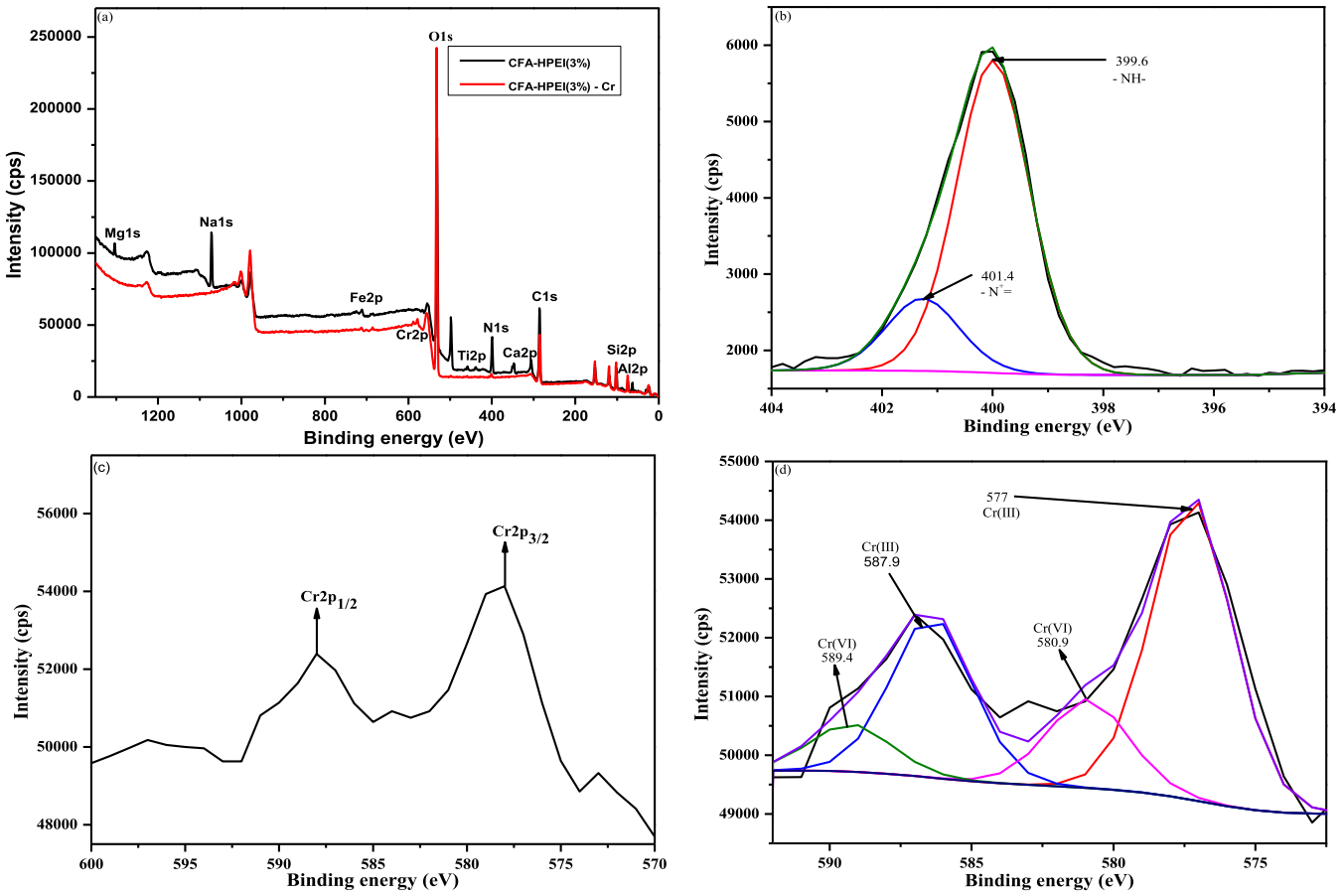

Figure 13. (a) XPS spectrum of CFA−HPEI (3%) adsorbent before and after Cr(VI) adsorption, (b) N 1s core level spectrum before adsorption, (c,d) Cr 2p core level spectrum after adsorption.

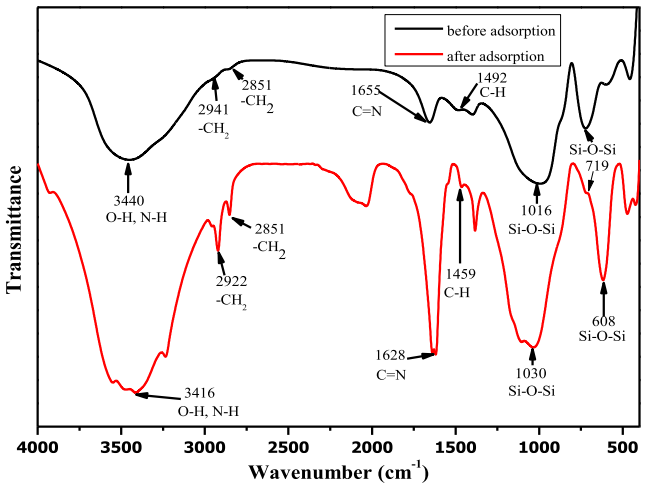

Figure 14. FTIR spectra of CFA−HPEI (3%) adsorbent before and after Cr(VI) adsorption.

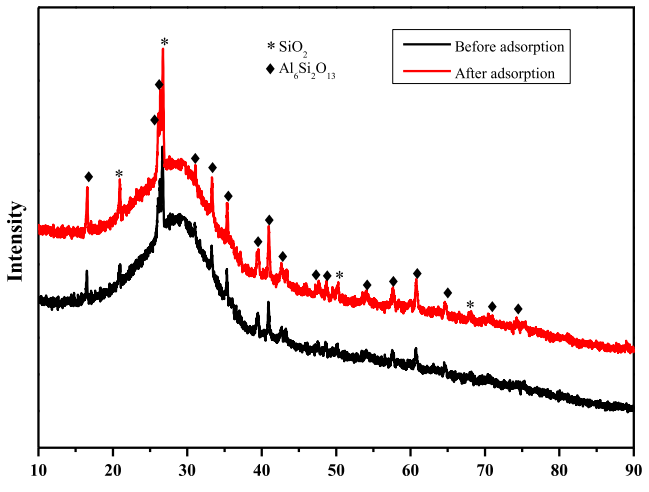

Figure 15. XRD spectra of CFA−HPEI (3%) adsorbent before and after Cr(VI) adsorption.

sulfur atoms of MB, and $\pi-\pi$ interactions between the aromatic structure of MB and the polymeric backbone of HPEI as well as the surface area of the adsorbent.[85,86] The results reveal that the presence of Cr resulted in improvement in the photocatalytic activity of the material. Cr is reported to be one of the key photocatalytic materials used in the area of cleaning up environmental pollutants.[37] According to the pseudo-first-order equation, the rates of MB photodegradation were found to be −0.01520 and −0.02527 min^{-1} for the clean and loaded adsorbent, respectively (Figure 17d). Table 9 depicts a comparison of the degradation of MB obtained in this study with other catalysts. The results show that the performance of the Cr-loaded CFA−HPEI (3%) adsorbent is comparable with that of the other catalysts studied. The adsorbent displayed good stability after degradation of MB. The FTIR and XRD illustrated no structural changes before and after application, as depicted in Figures S2 and S3. DRS analysis showed a slight decrease in band gap from 3.40 to 3.32 eV (Figures 16b and S4), confirming

https://doi.org/10.1021/acsomega.3c06491
ACS Omega 2024, 9, 8954−8972

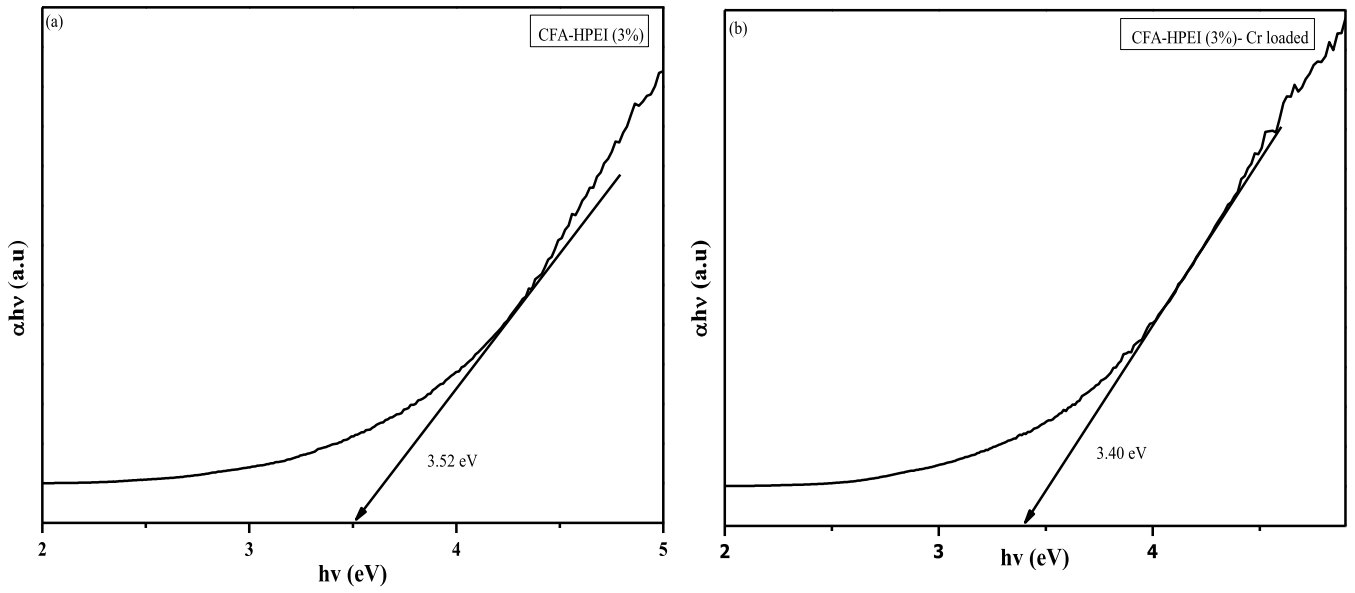

Figure 16. Tauc plots of (a) CFA−HPEI (3%) adsorbent and (b) Cr-loaded CFA−HPEI (3%) adsorbent.

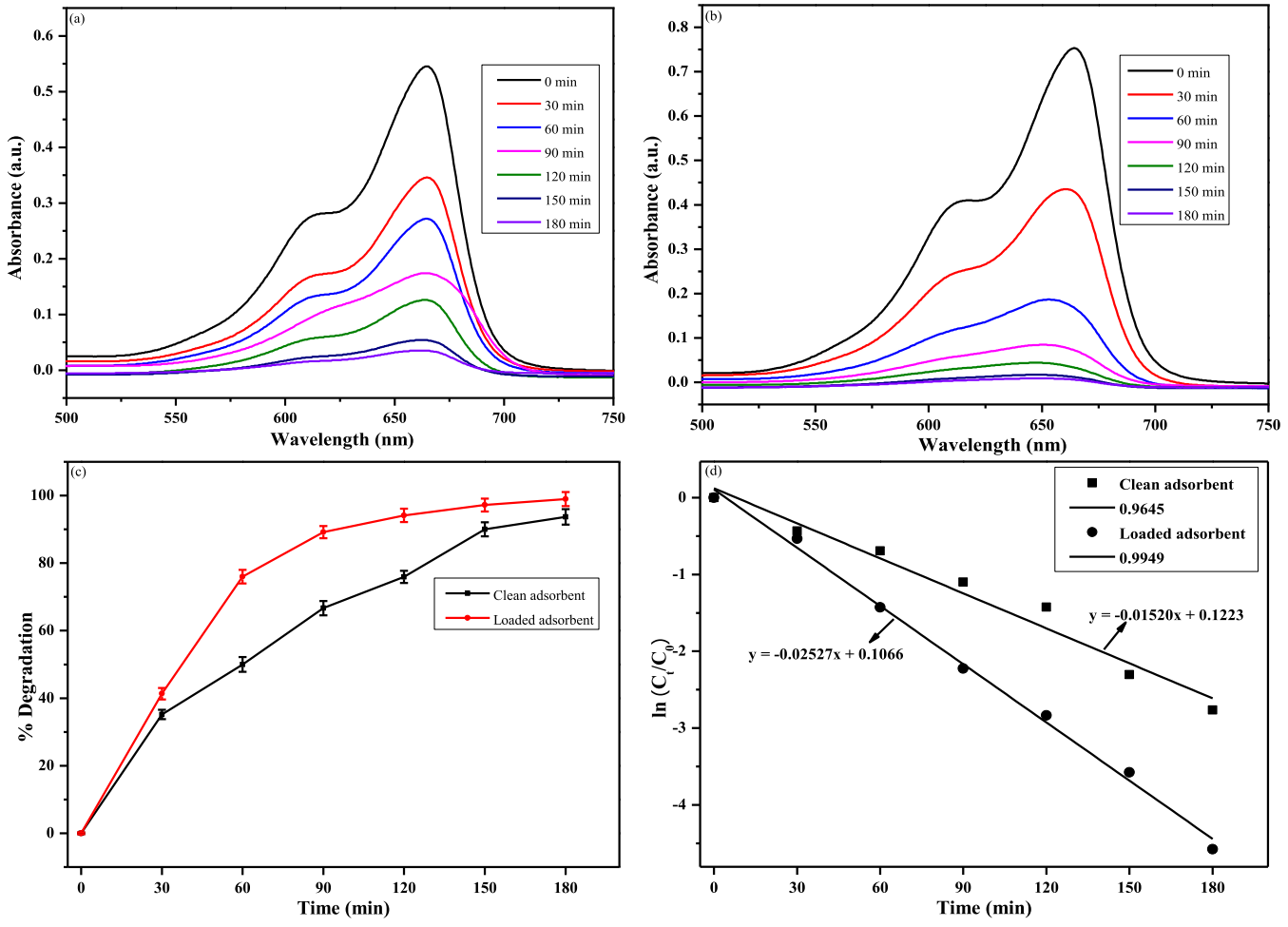

Figure 17. UV−vis spectra of photocatalytic degradation of MB by (a) CFA−HPEI (3%) adsorbent and (b) Cr-loaded CFA−HPEI (3%) adsorbent, and (c) percentage degradation of MB, and (d) rate constants.

good photocatalytic properties of the material. Moreover, no traces of Cr(VI) could be detected in the treated MB solution as confirmed by the absence of the absorbance peak associated with Cr(VI) at 540 nm (Figure S7).

3.2.9. Possible Mechanism for the Degradation of MB Using CFA−HPEI-Cr. As shown in Figure S5, the intensity of the MB peak appearing at a retention time of 5.1 min decreased as the irradiation time was prolonged, suggesting the successful

https://doi.org/10.1021/acsomega.3c06491
ACS Omega 2024, 9, 8954−8972

Table 9. Comparison of Percentage Degradation of MB by Cr-Loaded CFA−HPEI (3%) Adsorbent with Other Catalysts

no	catalyst	dye	degradation time (min)	degradation (%)	refs
1	CFA heterogeneous Fenton catalyst	MB	240	93.0	86
2	CFA-$CoFe_2O_4$	MB	60	99.0	87
3	3.7% anatase red mud geopolymer	MB	720	94.6	88
4	CFA-based zeolite NaP1	MB	720	96.0	89
5	CFA@$(r\text{-}GO/TNS)_8$	MB	70	55.0	90
6	$MnFe_2O_4$/coal fly ash nanocomposite	MB	30	100	91
7	coal fly ash based zinc ferrite (CFA/$ZnFe_2O_4$) composite	MB	60	97.0	92
8	CuO/CFA based zeolite Na-X	MB	180	80.2	93
9	Fe_2O_3−TiO_2/fly-ash-cenosphere composite	MB	60	86.81	94
10	CFA-HPEI−Cr adsorbent	MB	180	98.9	this work

degradation of MB in the presence of visible light. MS was used to detect the MB precursor mass and possible mass fragments resulting from the degradation process. The mass spectra of the samples collected after 30, 90, 150, and 180 min are given in Figure S6. The degradation of MB results in possible intermediate products with m/z of 270 (Azure B), 256 (Azure A), 242.2 (Azure C), and 228 (Thionin).[95] Figure S6 shows that after 90 min, the dominating mass is that of the precursor ion (284.1), while virtually none of the expected intermediate masses could be detected, suggesting that the MB could have disintegrated instead of following a slow and steady fragmentation process. This might be due to the presence of Cr since metals have large adsorption capability and also display strong photodegradation activity due to a decrease in electron−hole recombination. This leads to rapid degradation resulting in the intermediate masses not being detected in the solutions.[96] After visible light irradiation for 150 min, the precursor ion (284.1) has decreased with the appearance of a compound with m/z of 173. After 180 min, the complete degradation of the precursor ion is accompanied by the appearance of a compound with m/z of 173 and 234, which are possible intermediate products of Azure A (256), as depicted in Figure 18.

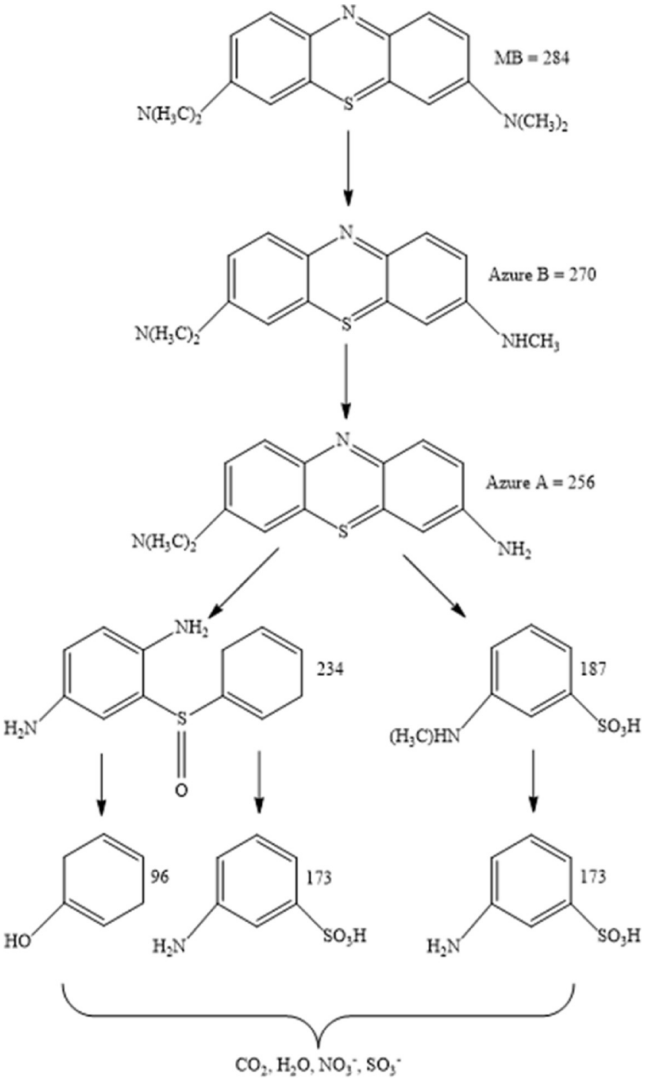

Figure 18. Possible degradation pathway of MB by Cr-loaded CFA−HPEI (3%) adsorbent.

4. CONCLUSIONS

A CFA-based adsorbent was prepared and evaluated for the remediation of Cr(VI) from water. The CFA−HPEI adsorbents were prepared by functionalizing the CFA with different HPEI loadings (1−5%). The adsorbents were characterized using XRF, XRD, XPS, SEM−EDS, FTIR, EA, and BET. The 3%-HPEI-loaded adsorbent performed best with a maximum adsorption capacity of 85.93 mg/g at pH 2. The pseudo-second-order kinetics model best defined the adsorption kinetics, and the Freundlich adsorption isotherm model best described the equilibrium adsorption data. The XPS confirmed the existence of both Cr(VI) and Cr(III) on the surface of the adsorbent, suggesting that the remediation of Cr(VI) occurred through the electrostatic attraction of Cr(VI) onto the adsorbent followed by the reduction of Cr(VI) to Cr(III) by the CFA−HPEI (3%) adsorbent. The Cr-loaded adsorbent was reused as a photocatalyst for the degradation of MB with 98.9% degradation accompanied by adsorption within 180 min. The Cr-loaded CFA−HPEI adsorbent displayed strong photodegradation activity as it resulted in rapid degradation of MB, which was accompanied by the detection of products with m/z of 173 and 234 corresponding to intermediate degradation of Azure A. Furthermore, there was no structural change in the FTIR and XRD analyses performed before and after application, indicating that the adsorbent exhibited good stability following the degradation of MB. This study showed that the HPEI-functionalized CFA could be utilized as an adsorbent for the removal of Cr(VI) from water. In order to prevent additional environmental pollution, the Cr-loaded adsorbent can also be reused as a photocatalyst for the degradation of MB. Based on the promising results obtained from this study, other hyperbranched polymers will be explored for the functionalization of CFA targeting different emerging pollutants (i.e., pharmaceuticals and personal care products) and other heavy metal ions prevalent in water and wastewater. As part of ongoing work, the

https://doi.org/10.1021/acsomega.3c06491
ACS Omega 2024, 9, 8954−8972

adsorbent will be supported on beads, which can be further used in columns for upscaling of the technology. This upscaled technology will then be tested against real water samples collected from pharmaceuticals, agricultural, and various manufacturing industries as HPEI polymers are effective in the removal of organic pollutants due to their hydrophobic cavities.

■ ASSOCIATED CONTENT

Supporting Information

The Supporting Information is available free of charge at https://pubs.acs.org/doi/10.1021/acsomega.3c06491.

Additional experimental details, methods, and figures (PDF)

■ AUTHOR INFORMATION

Corresponding Author

Soraya Phumzile Malinga − *Department of Chemical Sciences, University of Johannesburg, Doornfontein 2028, South Africa;* orcid.org/0000-0003-0139-9781; Email: smalinga@uj.ac.za

Authors

Molahlegi Orienda Sebabi − *Department of Chemical Sciences, University of Johannesburg, Doornfontein 2028, South Africa; Spectrum, University of Johannesburg, Auckland Park 2006, South Africa*

Nonhlangabezo Mabuba − *Department of Chemical Sciences, University of Johannesburg, Doornfontein 2028, South Africa;* orcid.org/0000-0003-0209-7451

Kriveshini Pillay − *Department of Chemical Sciences, University of Johannesburg, Doornfontein 2028, South Africa;* orcid.org/0000-0002-2134-7666

Complete contact information is available at: https://pubs.acs.org/10.1021/acsomega.3c06491

Notes

The authors declare no competing financial interest.

■ ACKNOWLEDGMENTS

The South Africa/India Joint Science and Technology Research Collaboration (IND190911475982), Water Research Commission(WRC project no.: K52488//3), National Research Foundation-Competitive Support for Unrated Researchers (NRF-CSUR:SRUG210407592746), Center for Nanomaterials Science Research (CNSR: University of Johannesburg), Faculty of Science (University of Johannesburg), and Spectrum (The Analytical Facility of the Faculty of Science, University of Johannesburg) are all acknowledged by the authors for their support.

■ REFERENCES

(1) Iloms, E.; Ololade, O. O.; Ogola, H. J. O.; Selvarajan, R. Investigating industrial effluent impact on municipal wastewater treatment plant in vaal, South Africa,. *Int. J. Environ. Res. Public Health* **2020**, *17* (3), 1096−1118.

(2) Das, R.; Hugues, K. P.; Maity, A. Surface-modified conducting polymer- based nanostructured materials for the removal of toxic heavy metals from wastewater. *Adv. Remed. Environ. Nanostruct. Mater.* **2019**, *25*, 112−136.

(3) Vareda, J. P.; Valente, A. J. M.; Durães, L. Assessment of heavy metal pollution from anthropogenic activities and remediation strategies : A review,. *J. Environ. Manage.* **2019**, *246* (May), 101−118.

(4) Zhou, L.; Chi, T.; Zhou, Y.; Lv, J.; Chen, H.; Sun, S.; Zhu, X.; Wu, H.; Hu, X. Efficient removal of hexavalent chromium through adsorption-reduction-adsorption pathway by iron-clay biochar composite prepared from Populus nigra,. *Sep. Purif. Technol.* **2022**, *285* (October 2021), 120386.

(5) Barad, J. M.; Kohli, H. P.; Chakraborty, M. Adsorption of hexavalent chromium from aqueous stream by maghemite nanoparticles synthesized by the microemulsion method,. *Energy Nexus* **2022**, *5*, 100035.

(6) Kar, S.; Equeenuddin, S. M. Adsorption of Hexavalent Chromium using Natural Goethite : Isotherm, Thermodynamic and Kinetic Study. *J. Geol. Soc. India* **2019**, *93* (3), 285−292.

(7) Tan, J.; Song, Y.; Huang, X.; Zhou, L. Facile functionalization of natural peach gum polysaccharide with multiple amine groups for highly efficient removal of toxic hexavalent chromium (Cr(VI)) ions from water,. *ACS Omega* **2018**, *3*, 17309−17318.

(8) Bhaumik, M.; Choi, H. J.; Seopela, M. P.; McCrindle, R. I.; Maity, A. Highly effective removal of toxic Cr(VI) from wastewater using sulfuric acid-modified avocado seed,. *Ind. Eng. Chem. Res.* **2014**, *53* (3), 1214−1224.

(9) EPA. *Effluent Standards*, 2012.

(10) Sinha, R.; Kumar, R.; Sharma, P.; Kant, N.; Shang, J.; Aminabhavi, T. M. Removal of hexavalent chromium via biochar-based adsorbents: State-of-the-art, challenges, and future perspectives,. *J. Environ. Manage.* **2022**, *317*, 115356.

(11) Adeiga, O. I.; Velempini, T.; Pillay, K. Polyaniline-decorated Macadamia nutshell composite: an adsorbent for the removal of highly toxic Cr(VI) and efficient catalytic activity of the spent adsorbent for reuse. *Polym. Bull.* **2022**, *80*, 1951−1973.

(12) Singh, S.; Wasewar, K. L.; Kansal, S. K. Low-cost adsorbents for removal of inorganic impurities from wastewater. *Inorganic Pollutants in Water*; INC, 2020; pp 173−203.

(13) Singh, N. B.; Nagpal, G.; Agrawal, S.; Rachna. Water purification by using Adsorbents: A Review,. *Environ. Technol. Innovat.* **2018**, *11*, 187−240.

(14) Yogeshwaran, V.; Priya, A. K. Experimental studies on the removal of heavy metal ion concentration using sugarcane bagasse in batch adsorption process,. *Desalin. Water Treat.* **2021**, *224*, 256−272.

(15) Hussain, S. T.; Ali, S. Removal of heavy metal by ion exchange using bentonite clay,. *J. Ecol. Eng.* **2021**, *22* (1), 104−111.

(16) Adilbekova, A. O.; Faizullayev, S.; Bayekenov, A.; Kujawski, W. The Effect of Fly Ash and Tween 20 Combination in Water-In-Crude Oil Emulsions Treatment,. *Eng. Sci.* **2023**, *25*, 27−30.

(17) Chassapis, K.; Roulia, M.; Vrettou, E.; Fili, D.; Zervaki, M. Biofunctional characteristics of lignite fly ash modified by humates: A new soil conditioner,. *Bioinorg. Chem. Appl.* **2010**, *2010*, 1−8.

(18) Musapatika, E. T.; Onyango, M. S.; Aoyi, O. Cobalt(II) removal from synthetic wastewater by adsorption on South African coal fly ash,. *S. Afr. J. Sci.* **2010**, *106* (9/10), 1−7.

(19) Park, J.; Bae, S. Highly efficient and magnetically recyclable Pd catalyst supported by iron-rich fly ash@fly ash-derived SiO_2 for reduction of p-nitrophenol,. *J. Hazard. Mater.* **2019**, *371* (February), 72−82.

(20) Troung, H. B.; Ike, I. A.; Sik, Y.; Hur, J. Polyethyleneimine modification of activated fly ash and biochar for enhanced removal of natural organic matter from water via adsorption,. *Chemosphere* **2020**, *243*, 1−9.

(21) Harja, M.; Lupu, N.; Chiriac, H.; Herea, D. D.; Buema, G. Studies on the Removal of Congo Red Dye by an Adsorbent Based on Fly-Ash@Fe_3O_4 Mixture,. *Magnetochemistry* **2022**, *8*, 125.

(22) Wang, Y.; Zhang, Y.; Liu, X.; Sun, S.; Qin, S.; Huang, J.; Chen, B. Polydopamine/β-cyclodextrin/coal fly ash composite for the highly efficient extraction of uranium from water environment. *J. Ind. Eng. Chem.* **2023**, *127*, 239−249.

(23) Wang, Z.; Xu, L.; Su, N.; Zhu, S.; Wu, D. Preparation of amino-functionalized fly ash based tobermorite for enhanced removal of Cr(VI),. *Environ. Sci. Pollut. Res.* **2023**, *30*, 54547−54555.

(24) Zeng, H.; Wang, L.; Zhang, D.; Yan, P.; Nie, J.; Sharma, V. K.; Wang, C. Highly efficient and selective removal of mercury ions using

hyperbranched polyethylenimine functionalized carboxymethyl chitosan composite adsorbent,. *Chem. Eng. J.* **2019**, *358* (September 2018), 253−263.
(25) Li, S.; Wu, M.; Lu, L.; Zhu, J. Removal of Cd(II) from water by HPEI modified humin,. *Sustain.* **2020**, *12* (19), 7931.
(26) Huang, Q. S.; Wu, W.; Wei, W.; Ni, B. J. Polyethylenimine modified potassium tungsten oxide adsorbent for highly efficient Ag^+ removal and valuable Ag0 recovery,. *Sci. Total Environ.* **2019**, *692*, 1048−1056.
(27) Chen, Y. W.; Yu, X.; Appiah-Hagan, E.; Pizarro, J.; Arteca, G. A.; Mercier, L.; Wei, Q.; Belzile, N. Utilization of coal fly ash and drinking water sludge to remove anionic As(V), Cr(VI), Mo(VI) and Se(IV) from mine waters,. *J. Environ. Chem. Eng.* **2018**, *6* (2), 2470−2479.
(28) Huang, X.; Zhao, H.; Zhang, G.; Li, J.; Yang, Y.; Ji, P. Potential of removing Cd(II) and Pb(II) from contaminated water using a newly modified fly ash,. *Chemosphere* **2020**, *242*, 125148.
(29) Truong, H. B.; Ike, I. A.; Ok, Y. S.; Hur, J. Polyethyleneimine modification of activated fly ash and biochar for enhanced removal of natural organic matter from water via adsorption,. *Chemosphere* **2020**, *243*, 125454.
(30) Xiao, Z.; Xie, Y.; Militz, H.; Mai, C. Effect of glutaraldehyde on water related properties of solid wood,. *Holzforschung* **2010**, *64* (4), 483−488.
(31) Balasubramanian, S.; Pugalenthi, V. Determination of total chromium in tannery waste water by inductively coupled plasma-atomic emission spectrometry, flame atomic absorption spectrometry and UV-visible spectrophotometric methods,. *Talanta* **1999**, *50* (3), 457−467.
(32) Gupta, M.; Gupta, H.; Kharat, D. S. Adsorption of Cu(II) by low cost adsorbents and the cost analysis,. *Environ. Technol. Innovat.* **2018**, *10*, 91−101.
(33) Sahoo, T. R.; Prelot, B. Adsorption processes for the removal of contaminants from wastewater. *Nanomaterials for the Detection and Removal of Wastewater Pollutants*; Elsevier Inc., 2020; pp 161−222.
(34) Wadhawan, S.; Jain, A.; Nayyar, J.; Mehta, S. K. Role of nanomaterials as adsorbents in heavy metal ion removal from waste water: A review,. *J. Water Process Eng.* **2020**, *33* (October 2019), 101038.
(35) Matouq, M.; Jildeh, N.; Qtaishat, M.; Hindiyeh, M.; Al Syouf, M. Q. The adsorption kinetics and modeling for heavy metals removal from wastewater by Moringa pods,. *J. Environ. Chem. Eng.* **2015**, *3*, 775−784.
(36) Doke, K. M.; Khan, E. M. Adsorption thermodynamics to clean up wastewater; critical review,. *Rev. Environ. Sci. Biotechnol.* **2013**, *12* (1), 25−44.
(37) Larbi, T.; Amara, M. A.; Ouni, B.; Amlouk, M. Enhanced photocatalytic degradation of methylene blue dye under UV-sunlight irradiation by cesium doped chromium oxide thin films,. *Mater. Res. Bull.* **2017**, *95*, 152−162.
(38) Kalombe, R. M.; Ojumu, T. V.; Katambwe, V. N.; Nzadi, M.; Bent, D.; Nieuwouldt, G.; Madzivire, G.; Kevern, J.; Petrik, L. F. Treatment of acid mine drainage with coal fly ash in a jet loop reactor pilot plant,. *Miner. Eng.* **2020**, *159* (August), 106611.
(39) Makgabutlane, B.; Nthunya, L. N.; Musyoka, N.; Dladla, B. S.; Nxumalo, E. N.; Mhlanga, S. D. Microwave-assisted synthesis of coal fly ash-based zeolites for removal of ammonium from urine,. *RSC Adv.* **2020**, *10* (4), 2416−2427.
(40) Potgieter, J. H.; Pearson, S.; Pardesi, C. Kinetic and thermodynamic parameters for the adsorption of methylene blue using fly ash under batch, column, and heap leaching configurations,. *Coal Combust. Gasif. Prod.* **2018**, *11*, 22−33.
(41) Wang, N.; Sun, X.; Zhao, Q.; Yang, Y.; Wang, P. Leachability and adverse effects of coal fly ash: A review,. *J. Hazard. Mater.* **2020**, *396* (January), 122725.
(42) Ojumu, T. V.; Du Plessis, P. W.; Petrik, L. F. Synthesis of zeolite A from coal fly ash using ultrasonic treatment - A replacement for fusion step,. *Ultrason. Sonochem.* **2016**, *31*, 342−349.
(43) Plessis, P.; Ojumu, T.; Petrik, L. Waste minimization protocols for the process of synthesizing zeolites from South African coal fly ash,. *Materials* **2013**, *6* (5), 1688−1703.
(44) Meng, R.; Lv, P.; Yang, Y.; Xu, D.; Gao, T.; Fu, Y. Low-temperature alkali-modified fly ash as an effective adsorbent for removal of ammonia nitrogen, phosphorus and COD from the wastewater,. *Earth Environ. Sci.* **2020**, *569* (1), 012026.
(45) Doucet, F. J.; Mohamed, S.; Neyt, N.; Castleman, B. A.; Van Der Merwe, E. M. Thermochemical processing of a South African ultrafine coal fly ash using ammonium sulphate as extracting agent for aluminium extraction. *Hydrometallurgy* **2016**, *166*, 174−184.
(46) Van Der Merwe, E. M.; Prinsloo, L. C.; Mathebula, C. L.; Swart, H. C.; Coetsee, E.; Doucet, F. J. Surface and bulk characterization of an ultrafine South African coal fly ash with reference to polymer applications,. *Appl. Surf. Sci.* **2014**, *317*, 73−83.
(47) Ononiwu, N. H.; Ozoegwu, C. G.; Akinribide, O. J.; Akinlabi, E. T. Effect of particle size on the microstructure and distribution of fly ash for metal matrix composite applications. *Mater. Today Proc.* **2021**, *44*, 1118−1123.
(48) Umejuru, E. C.; Prabakaran, E.; Pillay, K. Coal fly ash coated with carbon hybrid nanocomposite for remediation of cadmium (II) and photocatalytic application of the spent adsorbent for reuse,. *Results Mater.* **2020**, *7*, 100117.
(49) Dash, S.; Chaudhuri, H.; Udayabhanu, G.; Sarkar, A. Fabrication of inexpensive polyethylenimine-functionalized fly ash for highly enhanced adsorption of both cationic and anionic toxic dyes from water,. *Energy Fuels* **2016**, *30* (8), 6646−6653.
(50) Suzaimi, N. D.; Goh, P. S.; Malek, N. A. N. N.; Lim, J. W.; Ismail, A. F. Performance of branched polyethyleneimine grafted porous rice husk silica in treating nitrate-rich wastewater via adsorption,. *J. Environ. Chem. Eng.* **2019**, *7* (4), 103235.
(51) Ma, Y.; Liu, W. J.; Zhang, N.; Li, Y. S.; Jiang, H.; Sheng, G. P. Polyethylenimine modified biochar adsorbent for hexavalent chromium removal from the aqueous solution,. *Bioresour. Technol.* **2014**, *169*, 403−408.
(52) Woolard, C. D.; Petrus, K.; Van der Horst, M. The use of a modified fly ash as an adsorbent for lead. *Water SA* **2000**, *26* (4), 531−536.
(53) Geng, J.; Yin, Y.; Liang, Q.; Zhu, Z.; Luo, H. Polyethyleneimine cross-linked graphene oxide for removing hazardous hexavalent chromium : Adsorption performance and mechanism,. *Chem. Eng. J.* **2019**, *361* (August2018), 1497−1510.
(54) Zhao, Y.; Yang, S.; Ding, D.; Chen, J.; Yang, Y.; Lei, Z.; Feng, C.; Zhang, Z. Effective adsorption of Cr (VI) from aqueous solution using natural Akadama clay,. *J. Colloid Interface Sci.* **2013**, *395* (1), 198−204.
(55) Vakili, M.; Deng, S.; Liu, D.; Li, T.; Yu, G. Preparation of aminated cross-linked chitosan beads for efficient adsorption of hexavalent chromium,. *Int. J. Biol. Macromol.* **2019**, *139*, 352−360.
(56) Li, G.; Zhang, J.; Liu, J.; Chen, S.; Li, H. Investigation of the adsorption characteristics of Cr(VI) onto fly ash, pine nut shells, and modified bentonite,. *Desalin. Water Treat.* **2020**, *195*, 389−402.
(57) Li, L.; Fan, L.; Sun, M.; Qiu, H.; Li, X.; Duan, H.; Luo, C. Adsorbent for chromium removal based on graphene oxide functionalized with magnetic cyclodextrin-chitosan,. *Colloids Surf., B* **2013**, *107*, 76−83.
(58) Suzaimi, N. D.; Goh, P. S.; Malek, N. A. N. N.; Lim, J. W.; Ismail, A. F. Enhancing the performance of porous rice husk silica through branched polyethyleneimine grafting for phosphate adsorption,. *Arab. J. Chem.* **2020**, *13* (8), 6682−6695.
(59) Peydayesh, M.; Mohammadi, T.; Bakhtiari, O. Water desalination via novel positively charged hybrid nano fi ltration membranes filled with hyperbranched polyethyleneimine modified MWCNT,. *J. Ind. Eng. Chem.* **2019**, *69*, 127−140.
(60) Kera, N. H.; Bhaumik, M.; Pillay, K.; Ray, S. S.; Maity, A. Selective removal of toxic Cr(VI) from aqueous solution by adsorption combined with reduction at a magnetic nanocomposite surface,. *J. Colloid Interface Sci.* **2017**, *503*, 214−228.
(61) Jiang, X.; Fan, W.; Li, C.; Wang, Y.; Bai, J.; Yang, H.; Liu, X. Removal of Cr(VI) from wastewater by a two-step method of oxalic

https://doi.org/10.1021/acsomega.3c06491
ACS Omega 2024, 9, 8954−8972

acid reduction-modified fly ash adsorption,. *RSC Adv.* **2019**, *9* (58), 33949−33956.
(62) Li, L.; Xu, Y.; Zhong, D. Highly Efficient Adsorption and Reduction of Cr(VI) Ions by a Core-Shell Fe_3O_4@UiO-66@PANI Composite,. *J. Phys. Chem. A* **2020**, *124* (14), 2854−2862.
(63) Zhou, Q.; Yan, C.; Luo, W. Polypyrrole coated secondary fly ash-iron composites: novel floatable magnetic adsorbents for the removal of chromium (VI) from wastewater,. *Mater. Des.* **2016**, *92*, 701−709.
(64) Setshedi, K. Z.; Bhaumik, M.; Songwane, S.; Onyango, M. S.; Maity, A. Exfoliated polypyrrole-organically modified montmorillonite clay nanocomposite as a potential adsorbent for Cr(VI) removal,. *Chem. Eng. J.* **2013**, *222*, 186−197.
(65) Haghseresht, F.; Lu, G. Q. Adsorption characteristics of phenolic compounds onto coal-reject-derived adsorbents,. *Energy Fuels* **1998**, *12* (6), 1100−1107.
(66) Hamdaoui, O.; Naffrechoux, E. Modeling of adsorption isotherms of phenol and chlorophenols onto granular activated carbon. Part I. Two-parameter models and equations allowing determination of thermodynamic parameters,. *J. Hazard. Mater.* **2007**, *147* (1−2), 381−394.
(67) Saha, P.; Chowdhury, S. Insight into adsorption thermodynamics. *Thermodynamics* **2011**, *16*, 349−368.
(68) Deng, X.; Qi, L.; Zhang, Y. Experimental study on adsorption of hexavalent chromium with microwave-assisted alkali modified fly ash,. *Water. Air. Soil Pollut.* **2018**, *229* (1), 18.
(69) Zhou, Q.; Yan, C.; Luo, W. Polypyrrole coated secondary fly ash - iron composites : novel floatable magnetic adsorbents for the removal of chromium (VI) from wastewater,. *Mater. Des.* **2016**, *92*, 701−709.
(70) Masinga, T.; Moyo, M.; Pakade, V. E. Removal of hexavalent chromium by polyethyleneimine impregnated activated carbon: intra-particle diffusion, kinetics and isotherms,. *J. Mater. Res. Technol.* **2022**, *18*, 1333−1344.
(71) Pei, Y.; Li, M.; Li, W.; Su, K.; Chen, J.; Yang, H.; Hu, D.; Zhang, S. Cr(VI) removal by cellulose-based composite adsorbent with a double-network structure,. *Colloids Surf., A* **2021**, *625*, 126963.
(72) Fayazi, M.; Ghanbarian, M. One-pot hydrothermal synthesis of polyethylenimine functionalized magnetic clay for efficient removal of noxious Cr(VI) from aqueous solutions,. *Silicon* **2020**, *12* (1), 125−134.
(73) Wang, J.; Cao, R.; He, D.; Saleem, A. Facile preparation of polyethyleneimine modified activated sludge-based adsorbent for hexavalent chromium removal from aqueous solution,. *Sep. Sci. Technol.* **2021**, *56* (3), 498−506.
(74) Qiu, Y.; Zhang, Q.; Gao, B.; Li, M.; Fan, Z.; Sang, W.; Hao, H.; Wei, X. Removal mechanisms of Cr(VI) and Cr(III) by biochar supported nanosized zero-valent iron: Synergy of adsorption, reduction and transformation,. *Environ. Pollut.* **2020**, *265*, 115018.
(75) Aigbe, U. O.; Ukhurebor, K. E.; Onyancha, R. B.; Osibote, O. A.; Darmokoesoemo, H.; Kusuma, H. S. Fly ash-based adsorbent for adsorption of heavy metals and dyes from aqueous solution: a review,. *J. Mater. Res. Technol.* **2021**, *14*, 2751−2774.
(76) Zhang, S.; Shi, Q.; Korfiatis, G.; Christodoulatos, C.; Wang, H.; Meng, X. Chromate removal by electrospun PVA/PEI nanofibers : adsorption, reduction, and effects of co-existing ions,. *Chem. Eng. J.* **2020**, *387*, 124179.
(77) Zhao, X.; Zheng, J.; You, S.; Du, L.; Liu, C.; Chen, K.; Liu, Y.; Ma, L. Selective adsorption of Cr(VI) onto amine-modified passion fruit peel biosorbent,. *Processes* **2021**, *9* (5), 790.
(78) Bao, S.; Yang, W.; Wang, Y.; Yu, Y.; Sun, Y.; Li, K. PEI grafted amino-functionalized graphene oxide nanosheets for ultrafast and high selectivity removal of Cr(VI) from aqueous solutions by adsorption combined with reduction: Behaviors and mechanisms,. *Chem. Eng. J.* **2020**, *399*, 125762.
(79) Bhaumik, M.; Agarwal, S.; Gupta, V. K.; Maity, A. Enhanced removal of Cr (VI) from aqueous solutions using polypyrrole wrapped oxidized MWCNTs nanocomposites adsorbent,. *J. Colloid Interface Sci.* **2016**, *470*, 257−267.
(80) Briggs, D. X-ray photoelectron spectroscopy (XPS). *Handbook Adhesion*, 2nd ed.; Wiley, 2005; pp 621−622.
(81) Zhang, Y.; Ma, H. L.; Peng, J.; Zhai, M.; Yu, Z. Z. Cr(VI) removal from aqueous solution using chemically reduced and functionalized graphene oxide,. *J. Mater. Sci.* **2013**, *48* (5), 1883−1889.
(82) Nezar, S.; Cherifi, Y.; Barras, A.; Addad, A.; Dogheche, E.; Saoula, N.; Laoufi, N. A.; Roussel, P.; Szunerits, S.; Boukherroub, R. Efficient reduction of Cr(VI) under visible light irradiation using CuS nanostructures,. *Arab. J. Chem.* **2019**, *12* (2), 215−224.
(83) Afzal, M. Z.; Sun, X. F.; Liu, J.; Song, C.; Wang, S. G.; Javed, A. Enhancement of ciprofloxacin sorption on chitosan/biochar hydrogel beads,. *Sci. Total Environ.* **2018**, *639*, 560−569.
(84) Lum, P. T.; Foo, K. Y.; Zakaria, N. A.; Palaniandy, P. Ash based nanocomposites for photocatalytic degradation of textile dye pollutants: A review,. *Mater. Chem. Phys.* **2020**, *241* (March 2019), 122405−122424.
(85) He, Y.; Zhang, L.; An, X.; Han, C.; Luo, Y. Microwave assistant rapid synthesis MCM-41-NH2 from fly ash and Cr(VI) removal performance,. *Environ. Sci. Pollut. Res.* **2019**, *26* (30), 31463−31477.
(86) Dawadi, S.; Gyawali, K.; Katuwal, S.; Gupta, A.; Lamichhane, G.; Khadka, S.; Koirala, A. R.; Parajuli, N. Degradation of methylene blue using hydrothermally synthesized α -manganese oxide nanostructures as a heterogeneous Fenton catalyst,. *J. Nanomater.* **2022**, *2022* (0), 1−12.
(87) Nadeem, N.; Yaseen, M.; Rehan, Z. A.; Zahid, M.; Shakoor, R. A.; Jilani, A.; Iqbal, J.; Rasul, S.; Shahid, I. Coal fly ash supported CoFe2O4 nanocomposites: Synergetic Fenton-like and photocatalytic degradation of methylene blue,. *Environ. Res.* **2022**, *206* (September 2021), 112280.
(88) Kaya-Özkiper, K.; Uzun, A.; Soyer-Uzun, S. Red mud- and metakaolin-based geopolymers for adsorption and photocatalytic degradation of methylene blue: Towards self-cleaning construction materials,. *J. Clean. Prod.* **2021**, *288*, 1−11.
(89) Chen, Q.; Zhao, Y.; Qiu, Q.; Long, L.; Liu, X.; Lin, S.; Jiang, X. Zeolite NaP1 synthesized from municipal solid waste incineration fly ash for photocatalytic degradation of methylene blue,. *Environ. Res.* **2023**, *218*, 114873−114910.
(90) Chen, J. W.; Yuan, B.; Shi, J. W.; Yang, J. C. E.; Fu, M. L. Reduced graphene oxide and titania nanosheet cowrapped coal fly ash microspheres alternately as a novel photocatalyst for water treatment,. *Catal. Today* **2018**, *315* (August 2017), 247−254.
(91) Mushtaq, F.; Zahid, M.; Mansha, A.; Bhatti, I. A.; Mustafa, G.; Nasir, S.; Yaseen, M. $MnFe_2O_4$/coal fly ash nanocomposite: a novel sunlight-active magnetic photocatalyst for dye degradation,. *Int. J. Environ. Sci. Technol.* **2020**, *17* (10), 4233−4248.
(92) Nadeem, N.; Zahid, M.; Rehan, Z. A.; Hanif, M. A.; Yaseen, M. Improved photocatalytic degradation of dye using coal fly ash-based zinc ferrite (CFA/$ZnFe_2O_4$) composite,. *Int. J. Environ. Sci. Technol.* **2022**, *19* (4), 3045−3060.
(93) Subbulekshmi, N. L.; Subramanian, E. Nano CuO Immobilized Zeolite Photocatalyst from Coal Fly Ash for Visible Light Photo-degradation of Methylene Blue without H_2O_2. *J. Pharm. Chem. Biol. Sci.* **2018**, *6*, 85−96.
(94) Zhu, J.; Liu, S.; Ge, J.; Guo, X.; Wang, X.; Wu, H. Synthesis of Fe_2O_3-TiO_2/fly-ash-cenosphere composite and its mechanism of photocatalytic oxidation under visible light,. *Res. Chem. Intermed.* **2016**, *42* (4), 3637−3654.
(95) Rauf, M. A.; Meetani, M. A.; Khaleel, A.; Ahmed, A. Photocatalytic degradation of Methylene Blue using a mixed catalyst and product analysis by LC/MS,. *Chem. Eng. J.* **2010**, *157* (2−3), 373−378.
(96) Matsunami, D.; Yamanaka, K.; Mizoguchi, T.; Kojima, K. Comparison of photodegradation of methylene blue using various TiO_2 films and WO_3 powders under ultraviolet and visible-light irradiation,. *J. Photochem. Photobiol. A Chem.* **2019**, *369* (July 2018), 106−114.

https://doi.org/10.1021/acsomega.3c06491
ACS Omega 2024, 9, 8954−8972